Prediction of Case Temperature of Axial Piston Pumps

Master's Thesis in Solid and Fluid Mechanics

DANIEL GRÖNBERG

Department of Applied Mechanics
Division of Fluid Dynamics
CHALMERS UNIVERSITY OF TECHNOLOGY
Göteborg, Sweden 2011
Master's Thesis 2011:62

Prediction of Case Temperature of Axial Piston Pumps

Master's Thesis in Solid and Fluid Mechanics
DANIEL GRÖNBERG

Department of Applied Mechanics
Division of Fluid Dynamics
CHALMERS UNIVERSITY OF TECHNOLOGY
Göteborg, Sweden 2011

Prediction of Case Temperature of Axial Piston Pumps
DANIEL GRÖNBERG

Prediction of Case Temperature of Axial Piston Pumps
Master's Thesis in Solid and Fluid Mechanics
DANIEL GRÖNBERG
Department of Applied Mechanics
Division of Fluid Dynamics
Chalmers University of Technology

Abstract

It is very important to be able to simulate axial piston pumps in order to understand its impact on the velocity, pressure and temperature of the lubricating oil in the pump. These variables have huge impact on the leakage in the lubricating gaps which is strongly related to the amount of power loss in the pump.

This thesis main focus have been to further develop a in-house developed FSI (Fluid Structure Interacting model) software called *CASPAR*, which is developed by *MAHA Fluid Power Research Center* in order to calculate the velocity, pressure and temperature in an axial piston pump.

This software has been further developed in three main research steps. One step was to develop a simplified and fast model that predicts the case temperature in an axial piston pump. The case temperature has previously been proven to have an impact on the power loss due to thermal deformation of the structure in the lubricating gaps. The calculated case temperature with this model should be used as a mixed boundary condition in the calculation tool *CASPAR*. The case temperature was previously taken from measurements.

Measurements regarding the case temperature in an actual axial piston pump has been taken in order to analyze and validate the developed model for the case temperature.

The behavior of the model has shown that the gap height is strongly influenced by the case temperature, hence the simplification to use constant gap heights in the lubricating gaps are not a valid approximation. Instead a further investigation has to be done and a recommendation to integrate the developed model with *CASPAR*, where both gap heights and leakage are calculated.

CASPAR is divided into two parts, the *Pressure Module* and *Gap Flow Module*. These have been further developed in this thesis in order to improve the efficiency and accuracy of the calculations of axial piston pumps. This was done by using and merging previous versions of the *Pressure Module* in to one single version and to develop the possibility to simulate the three lubricating gaps in an axial piston pump simultaneously with the *Gap Flow Module*.

The new single version of the *Pressure Module* is called the *Coupled Pressure Module* and it is now possible to run simulations while combining different models considering different physical effects. The simultaneous calculations of the lubricating gaps is called the *Coupled Gap Flow Module*. This has improved the time efficiency compared to independently calculated lubricating gaps. Friction forces are transmitted between the gaps in the way it is meant to be and the *Coupled Pressure Module* and *Coupled Gap Flow Module* is a part of the step against the development of the new version of *CASPAR*.

The new version of *CASPAR* should be one improved version where more physics is included compared to the old versions.

Keywords: Coupling, Axial piston pump, CASPAR, Leakages, Gap heights, Power loss, Case temperature, Model

Contents

Preface

In this thesis there have been three main research steps to improve the fluid structure interaction model calculation software *CASPAR*. These steps have improved the efficiency of the software as well as the user friendliness.

The work has been carried out from January to June 2011 at the Department of Agriculture and Biological engineering/Mechanical engineering, Division of Fluid Power, Purdue University, US, with supervisor Professor Monika Ivantysynova. The examiner to this work is Professor Lars Davidson at Chalmers University of Technology

Acknowledgements

I want to thank my supervisor Professor Monika Ivantysynova for her support. A special thanks to Andrew Schenk, Marco Zecchi, Matteo Pelosi and Richard Klop for their support during my work with *CASPAR* and to Michael Sprengel and Marco Zecchi again for setting up the test rig and for the introduction to take measurments. At last I want to thank Professor Lars Davidson.

Lafayette June 2011
Daniel Grönberg

1 Introduction

The main source of power loss in an axial piston machine is the lubricating gaps. The power loss due to viscous friction and gap flow occur in these lubricating interfaces. These are located between the cylinder block and valve plate, piston and cylinder, and between slipper and swash plate. It is very important to take this into account when the pump is designed.

A fluid structure interacting model called *CASPAR* has been developed. *CASPAR* is able to calculate displacement chamber pressure and losses due to viscous friction and gap flow [2].

CASPAR is divided into two modules, *Pressure Module* and *Gap Flow Module*. The *Pressure Module* calculates the instantaneous pressure in the displacement chamber, while the *Gap Flow Module* solves the leakage flows in the lubricating gaps.

CASPAR was developed by Monika Ivantysynova and Uwe Wieczorek in 2002. The software is still under development by the *CASPAR* team led by Professor Monika Ivantysynova at MAHA Fluid Power Research Center at Purdue University.

There have been many different versions of the *Pressure Module* developed for different purposes, i.e. different models considering different physical effects on different levels. The goal of the presented thesis work was to study the different mathematical models and to combine them in one large coupled program version. This will allow the user to combine effects and therefore to always use the most appropriate model for the given task. The *Coupled Pressure Module* (CPM) has been developed for this purpose.

The *Gap Flow Module* calculates the pressure, temperature fields, resulting flow and viscous friction in the three gaps (gap between moving piston and cylinder, gap between rotating cylinder block and valve plate and gap between rotating slipper and swash plate) independent from each other. However, the fluid film behavior of each of those gaps are connected and influenced by fluid forces generated in each gap. Therefore accurate results require a data exchange between these separate gap modules. By solving three interfaces simultaneously a better calculation of the flow field in the gap can be achieved, which is very important in order to determine the gap flow parameter and resulting pump performance data accurately. The development of *Coupled Gap Flow Module* (CGFM) has been the second research task of the presented thesis.

The temperature in the case of the pump is a critical parameter in order to calculate the temperature distribution in the solid parts and the temperature field in the fluid film. This is important in order to determine the resulting thermal deformations of the solid parts, which is influencing the amount of power loss due to the leakage flow and viscous friction. This temperature has previously been taken from measurement data. This becomes a problem when designing new pumps where no measurements are available. The case temperature affects the temperature in the gaps and thermal deformation of the solid parts in the axial piston machine. As a third research task of this thesis a model has been developed to calculate the case temperature prior to *CASPAR* to get a more accurate simulation of the leakage flows.

1.1 Purpose

The purpose of this project is to further improve the fluid structure interaction model *CASPAR* which has been developed by researchers of the Maha Fluid Power research Center. In particular the research focus on the following three steps.

1. Study and merge the various versions of models to predict the instantaneous cylinder pressure in axial piston machines. The new Pressure module should include the same

outputs as the various existing in-house models.

2. Develop a model that allows to run simulations for all three main lubricating interfaces of a swash plate type axial piston pump simultaneously by using the recently developed fluid structure interaction models. Also investigate how the power loss is affected due to the fluid forces that are transmitted between the three interfaces.

3. Develop a model that predicts the temperature in the pump casing. Also investigate how the gap heights are affecting the developed model.

1.2   Limitations

The CGFM was made as an external program that acts as a parent program for the three *Gap Flow Module* programs.

The model for the case temperature calculation is based on estimated values of dissipated energy and empirically chosen gap heights. It has therefore a limited accuracy. The model was carried out and verified with measurements of a Sauer-Danfoss 75cc pump.

1.3   Approach

CPM and CGFM were developed in Microsoft Visual Studio 2008 in the programming language C++. The case temperature model was made in MATLAB.

1.4   Sustainable development

To have simulation tool that calculates the fluid film, resulting fluid flow and viscous friction accurately in a pump is crucial when designing a pump. Digital prototyping does not only allow for better and less costly pump design. It also gives better inside and understanding of the influence of design parameters on pump performance, and reliability. It will allow for sustainable design and save costs of currently used trial and error design process.

2   Axial Piston Machines

An *Axial piston machine* is a positive displacement machine that works on the displacement principle[3]. The different types of displacement machines are divided in five main classifications, *Piston machines*, *Gear machines*, *Screw machines*, *Vane machines* and *other machines*. Most of the machines can operate either as a pump or a motor.

The *Piston machines* use moving pistons to displace fluid. The displacement chamber is formed between the cylinder and the moving piston. In axial piston machines the main movement of the piston is in axial direction. The main components of axial piston machine are the cylinder block, valve plate, swash plate, pistons, slippers and the pump case and shaft with shaft bearings, see Figure 2.1.

The cylinder block contains cylinder bores arranged on a circle with radius R_B. The piston move in axial direction between the inner and outer piston dead center while the cylinder block rotates and the pistons are supported on the inclined swash plate. The pistons need to be in continuous contact with the swash plate. In most pumps the piston are supported on the swash plate using slippers. The slipper are constructed in a way that allows to rotate around its own axis. The cylinder block is connected to a driving shaft. The cylinder block rotates with the shaft while the swash plate is stationary. Please note that there are designs with inverse kinematics, i.e. rotating swash plate and stationary cylinder block.
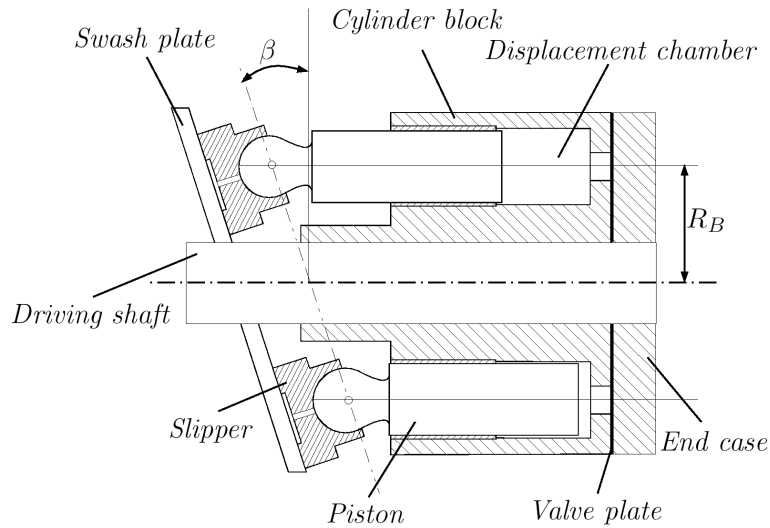
Figure 2.1: Parts of an axial piston machine swash plate design

Figure [2.2] explains the operation of an ideal pump when compressibility of the fluid is considered.
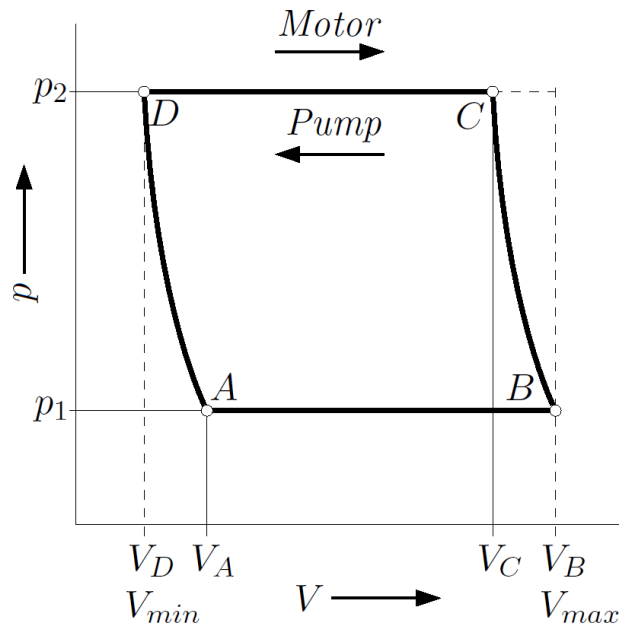

Figure 2.2: operational cycle of a ideal displacement machine with compressibility of a real fluid

When operating as a pump the flow will enter the displacement chamber at point A from the low pressure line at the inlet by the stroke of the piston. The displacement volume will increase until point B where the maximum volume V_{max} is achieved. The direction of the translatory piston movement will change direction and compress the fluid inside the displacement chamber until point C. The compression happen so fast that an adiabatic process is assumed [3]. The fluid will flow out to the outlet in the high pressure line until point D where the minimum volume V_{min} is achieved. The pressure falls because of the reversal movement of the piston until point A where the cycle is repeated.

If the axial piston machine operates as a motor, the flow will instead enter at the high pressure line at point D. The displacement chamber volume is increased until point C where the pressure suddenly falls to point B because of the expansion of the fluid. The displacement chamber opens to the low pressure line at the outlet where the fluid flows out

until point A. The displacement chamber closes to the outlet and the fluid is compressed because of the further reduction of the displacement chamber volume until point D. The cycle is then repeated.

The flow direction can be changed by either changing the displacement of the swash plate to either negative or positive angle or by changing the rotation direction of the driving shaft.

The *Axial piston machine* has two different classifications, *Swash plate* or *Bent axis* design. The main difference of these two pump types is where the torque is generated. The torque is generated on the cylinder block for a swash plate type pump, while for a bent axis pump it is generated on the driving flange [3], see Figure 2.3.
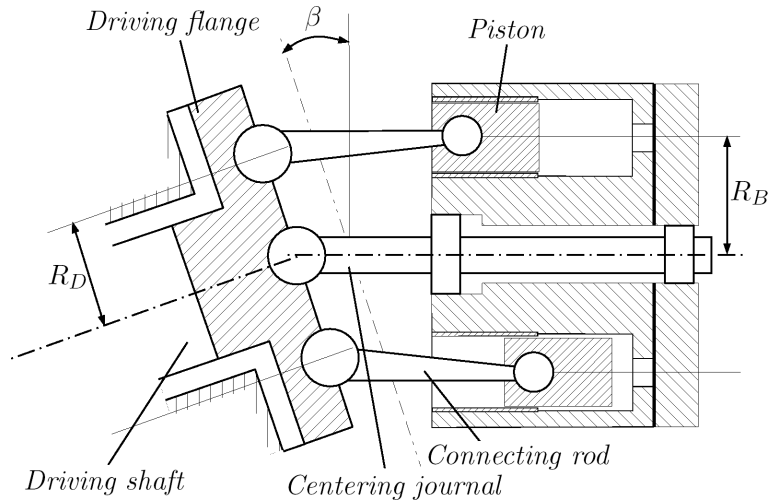

Figure 2.3: Parts of an axial piston machine bent axis design

The Bent axis type of machine has often an angle (β) of the cylinder block to the drive shaft. This enables the pump to operate with a bent axis/shaft, instead of the straight shaft in the swash plate design.

An axial piston pump with the swash plate design operating in pumping mode will be considered in this thesis, unless otherwise stated.

2.1 Lubricating gaps

The lubricating gaps function is to seal the displacement chamber [7] and to transfer high forces from one part to the other pump part, i.e. the gaps fulfills a sealing and bearing function. It also reduces friction and wear between the mobile parts [6]. An optimal design of these gaps is achieved when energy dissipation is minimum and the sealing and bearing functions are fulfilled under all pump operating conditions.

The lubricating interfaces in an axial piston pump are between the piston and cylinder, slipper and swash plate and the cylinder block and valve plate, see Figure 2.4. The lubricating gaps has been proven to bethe main sources of the power loss inside the pump.

The geometry of the gap has a big impact on the volumetric efficiency of the pump. The gap geometry depends on many things, such as pump speed, pressure and temperature.

The volumetric efficiency is the ratio between the effective pump flow (theoretical flow rate minus volumetric loss) and the theoretical flow rate, i.e.

$$\eta_v = \frac{Q_e}{Q_i} = \frac{Q_i - Q_s}{Q_i} \tag{2.1}$$

The volumetric efficiency is varying with pressure and pump speeds as in Figure 2.5.
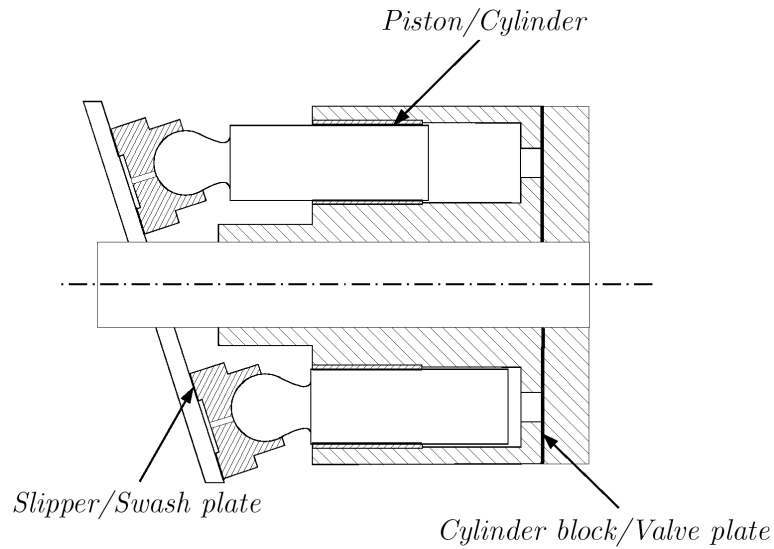
Figure 2.4: The lubricating interfaces in an axial piston pump
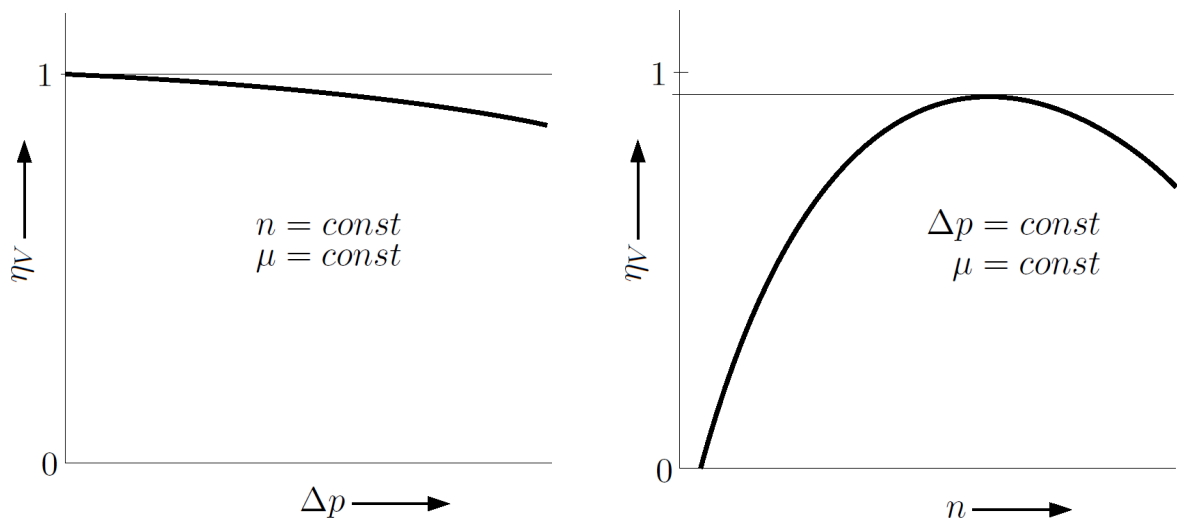
Figure 2.5: Volumetric efficiency of a pump for changing pressure or pump speed.

The power loss generated by the fluid flow in the lubricating gaps is

$$P_{loss} = P_{SQ} + P_{Sv} = Q_{leak}\Delta p + \mathbf{F} \bullet \mathbf{v} \qquad (2.2)$$

where P_{SQ} and P_{Sv} are power loss due to leakage flow and viscous friction respectively and $\mathbf{v}$ stands for the velocity of the fluid in the lubricating gap for the respective friction force, $\mathbf{F}$.

2.2 Kinetics of the pump

The schematic in Figure 2.6 represents an axial piston pump of swash plate design with cylinder bores parallel to the shaft.

Figure 2.6: Scheme of an axial piston pump of swash plate design

The rotation of the shaft is around the z-axis and the angular rotation speed, ω, is constant for all revolutions. The displacement of the piston, s_K, is in the z-axis direction.
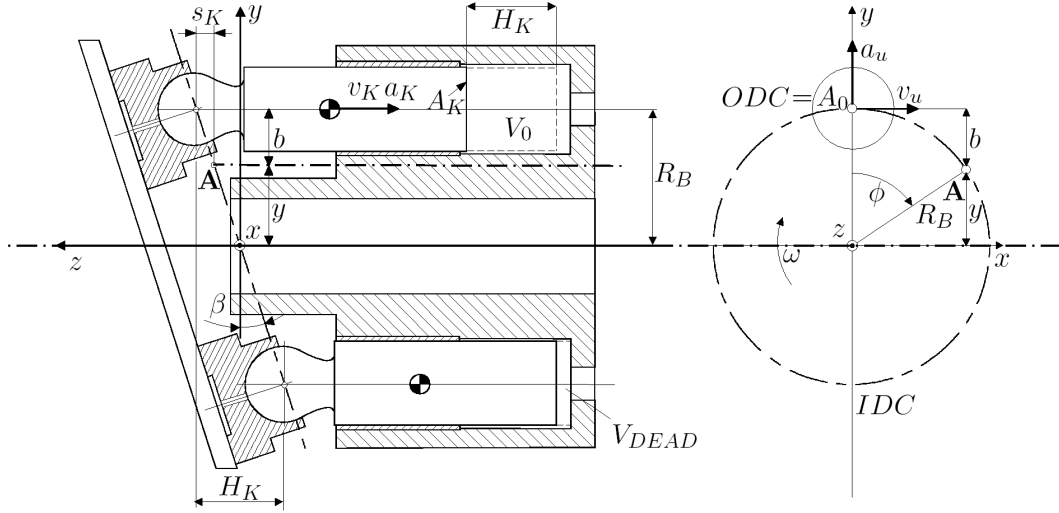
$$s_K = -z \tag{2.3}$$

The displacement depends on the pitch radius, R_B, and the location of the piston in ϕ-direction.

$$z = b \tan \beta \tag{2.4}$$

$$b = R_B - y \tag{2.5}$$

$$y = R_B \cos \phi \tag{2.6}$$

Combining Equations 2.3- 2.6 the following expression for the displacement is achieved

$$s_K = -R_B \tan \beta (1 - \cos \phi) \tag{2.7}$$

The maximum value of the displacement s_K is achieved after a half revolution when the piston is at $\phi = 180°$, this location is also referred to the inner dead center (IDC).

$$H_K = 2 R_B \tan \beta \tag{2.8}$$

The relative velocity of the piston in z-direction is

$$v_K = \frac{ds_K}{dt} = \frac{ds_K}{d\phi} \frac{d\phi}{dt} = \frac{ds_K}{d\phi} \omega \tag{2.9}$$

The derivative with respect of the angle ϕ of Equation 2.7 is

$$\frac{ds_K}{d\phi} = -R_B \tan \beta \sin \phi) \tag{2.10}$$

inserting Equation 2.10 into Equation 2.9 will yield the relative velocity

$$v_K = -\omega R_B \tan \beta \sin \phi = -\frac{1}{2}\omega H_K \sin \phi \tag{2.11}$$

The acceleration of the piston is

$$a_K = \frac{dv_K}{dt} = \frac{dv_K}{d\phi}\frac{d\phi}{dt} = \frac{dv_K}{d\phi}\omega \tag{2.12}$$

By taking the derivative of Equation 2.11 with respect of ϕ and inserting in Equation 2.12 will give

$$a_K = -\omega^2 R_B \tan \beta \cos \phi = -\frac{1}{2}\omega^2 H_K \cos \phi \tag{2.13}$$

The circumferential speed of the piston due to the rotation of the cylinder block is

$$v_u = R_B \omega \tag{2.14}$$

and the radial acceleration can then be expressed as

$$a_u = R_B \omega \tag{2.15}$$

The volume in the displacement chamber is continuously changing due to the linear motion of the piston, the rate of change of the volume is expressed as

$$\frac{dV}{dt} = v_K A_K = -\omega R_B A_K \tan \beta \sin \phi = -\frac{1}{2}\omega H_K \sin \phi A_k \tag{2.16}$$

where A_K is the area of the piston.

The volume in the displacement chamber is defined as

$$V_{DC} = V_0 - V = V_0 - s_K A_K = V_0 + R_B \tan \beta (1 - \cos \phi) A_K \tag{2.17}$$

where V_0 is the volume at the pistons outer dead center (ODC), i.e most outer point of the piston at $\phi = 0°$. The volume entrapped in the displacement chamber at IDC is called V_{DEAD}, and is the smallest achievable volume in the displacement chamber.

2.3 Forces at the piston

The external forces that act at the piston can be viewed in Figure 2.7. The F_{DK} force is the force created due to the pressurization of the displacement chamber.
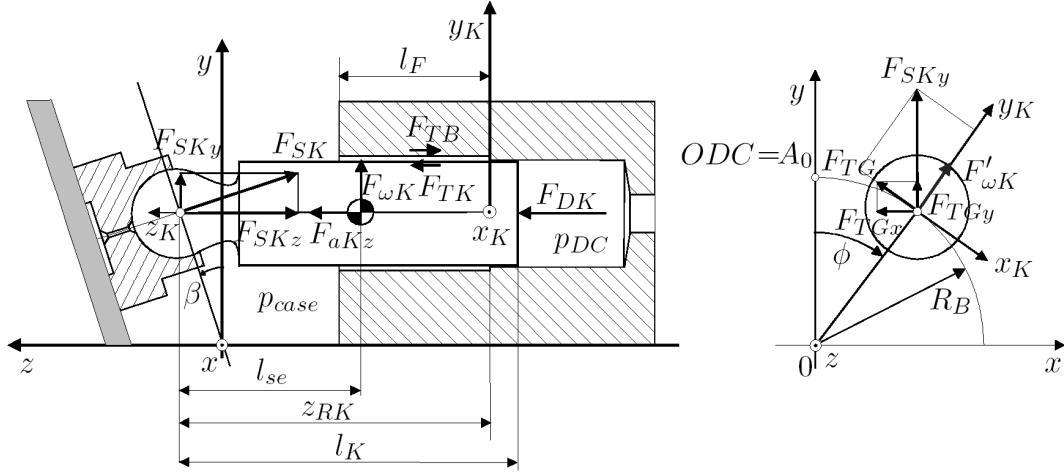

Figure 2.7: Forces acting at the piston

$$F_{DK} = A_k(p_{DC} - p_{case}) \tag{2.18}$$

The inertial force F_{aKz} is the force created due to the acceleration of the piston with slipper

$$F_{aKz} = -m_K a_K \tag{2.19}$$

The frictional force exerted on the piston is denoted as F_{TK}. This force can be divided into two components, one acting as a resiting force against the movement of the piston in the axial direction, F_{TKz} and the other one in the circumferential direction around the piston, F_{TKy}. These forces can be computed by calculating the integral of the shear stress due to the lubricating oil in the gap under the assumption of viscous friction (sufficient oil film in the gap [3]).

$$F_{TKz} = \int_A \tau_{yz} dA = \int_A \mu \frac{\partial v_z}{\partial y} dA \tag{2.20}$$

$$F_{TKy} = \int_A \tau_{yx} dA = \int_A \mu \frac{\partial v_y}{\partial y} dA \tag{2.21}$$

The total force acting on the piston in the axial direction is represented as F_{AKz}

$$F_{AKz} = F_{DK} + F_{aKz} + F_{TKz} \tag{2.22}$$

This force is transmitted to the slipper as a force perpendicular to the swash plate, F_{SK}. The reaction force from the swash plate will then act on the piston in the opposite direction, hence

$$F_{SK} = -\frac{F_{AKz}}{\cos \beta} \tag{2.23}$$

This is split up into two components

$$F_{SKy} = F_{AKz} \tan \beta \tag{2.24}$$

$$F_{SKz} = -F_{AKz} \tag{2.25}$$

The F_{SKz} is taken up by the cylinder block through the piston guide. The centrifugal force acting on the piston is denoted as $F_{\omega K}$.

$$F_{\omega K} = m_K a_u \tag{2.26}$$

The piston is also loaded by the frictional force, F_{TG}, that is transmitted from the slipper. The total external forces is described in a coordinate system that is fixed to the rotation of the piston around the shaft with angle ϕ. The y_K axis is pointing outward aligned with the centrifugal force, and the x_K axis is pointing from the center of the piston in the velocity direction of the piston. The origin of the system is aligned at the edge of the bushing at the chamber side, see Figure 2.7. The total external forces acting at the piston in the x_K and y_K-direction is then defined as

$$F_{Kx} = -F_{SKy} \sin \phi + F_{TG} \tag{2.27}$$

$$F_{Ky} = F_{SKy} \cos \phi + F_{\omega K} \tag{2.28}$$

where sufficient liquid film between the slipper and swash plate is assumed.

The external moments about the x_K and y_K axis are

$$M_{Kx} = -z_{RK} F_{SKy} \cos \phi - (z_{RK} - l_{SK}) F_{\omega K} \tag{2.29}$$

$$M_{Ky} = z_{RK} F_{Kx} \tag{2.30}$$

The external forces F_{Kx}, F_{Ky} and moments M_{Kx}, M_{Ky} are balanced with forces that is created due to the pressure distribution in the lubricant in order for the piston to be in equilibrium. The fluid forces are defined as the summation of the pressure times the area the pressure is acting upon in every point in the lubricant around the piston surface inside the bushing.

$$F_{fK} = \int_A p \, dA \tag{2.31}$$

This force is divided into two components in the reference system (x_K, y_K, z_K).

$$F_{fKx} = -F_{fK} \cos \phi_K \tag{2.32}$$

$$F_{fKy} = -F_{fK} \sin \phi_K \tag{2.33}$$

In the same way as for the external forces, the moments resulting from the pressure field are

$$M_{fKx} = F_{fKx} z_K \tag{2.34}$$

$$M_{fKy} = -F_{fKy} z_K \tag{2.35}$$

The external forces are balanced with the fluid forces at the piston to achieve equalibrium. The moments are transferred to forces that is also acting at the piston.

2.4 Forces at the slipper

The slipper can only transmit normal forces to the swash plate, this is due to the sliding bearing and the ability to rotate around its own axis.
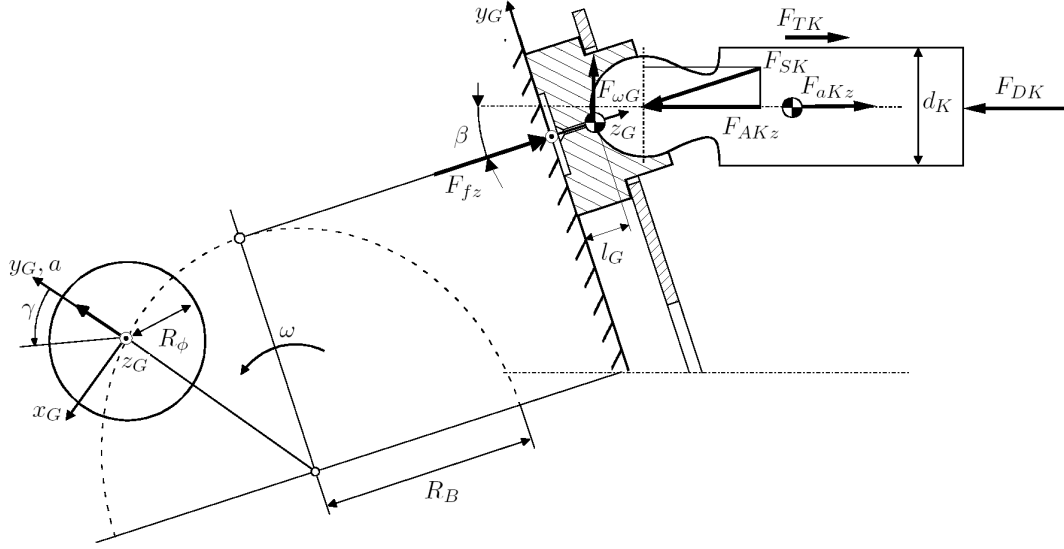

Figure 2.8: Forces acting at the slipper

The coordinate system applied in the slipper originates from its center and its plane agrees with the tilting of the swash plate angle β. The external force that is pressing the slipper to the swash plate is defined as

$$F_{KS} = \frac{F_{AKz}}{\cos \beta} \tag{2.36}$$

which is the same as F_{SK} but with opposite sign.

The arising firctional force, F_{TG}, is due to the rotational and sliding motion of the slipper on the swash plate. It can be determined under the assumption of viscous friction between the slipper and swash plate as the resultant force of the two components F_{TGx} and F_{TGy}

$$F_{TG} = \sqrt{F_{TGx}^2 + F_{TGy}^2} \tag{2.37}$$

where the components are computed as

$$F_{TGx} = \int_0^{2\pi} \int_{a_1}^{a_2} \tau_{zx} a \, da d\gamma = \int_0^{2\pi} \int_{a_1}^{a_2} \left(\tau_{za} \sin \gamma + \tau_{z\gamma} \cos \gamma \right) a \, da d\gamma \tag{2.38}$$

$$F_{TGy} = \int_0^{2\pi} \int_{a_1}^{a_2} \tau_{zy} a \, da d\gamma = \int_0^{2\pi} \int_{a_1}^{a_2} \left(\tau_{za} \cos \gamma - \tau_{z\gamma} \sin \gamma \right) a \, da d\gamma \tag{2.39}$$

The shear stresses in the cartesian coordinate system is divided into two components each in the local cylindrical polar coordinate system for the slipper, as shown in Figure 2.9.

$$\tau_{za} = \mu \frac{\partial v_a}{\partial z} \qquad \tau_{z\gamma} = \mu \frac{\partial v_\gamma}{\partial z} \tag{2.40}$$

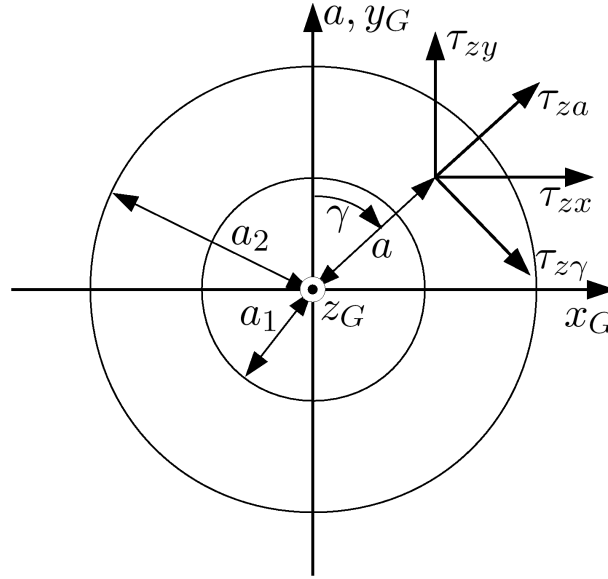The moment around the x-axis is as a result of the centrifugal force, $F_{\omega G}$

Figure 2.9: Shear stress components acting at a element on the slipper.

$$M_{Gx} = F_{\omega G} l_G \cos \beta = m_S R_B \omega^2 l_G \cos \beta \tag{2.41}$$

and the moment around the y-axis as a result of the frictional force F_{TG}, and is expressed as

$$M_{Gy} = F_{TGx} l_G \tag{2.42}$$

The corresponding fluid forces in the gap are expressed as

$$F_{Gfz} = \int_A p \, dA \tag{2.43}$$

$$M_{Gfx} = \int_A pa \, dA \tag{2.44}$$

$$M_{Gfy} = \int_A pa \, dA \tag{2.45}$$

The external and fluid moments are transferred to forces. The three fluid forces will be balanced by the external forces at the slipper.

2.5 Forces at the cylinder block

The external forces at the cylinder block can be viewed in Figure 2.10. The cylinder block is loaded with a pressure force, p_{DCi}, in the displacement chamber

$$F_{DBi} = -p_{DCi} A_D \tag{2.46}$$

where index i stands for one piston. The centrifugal force on the piston is transferred to the cylinder block through the following equation

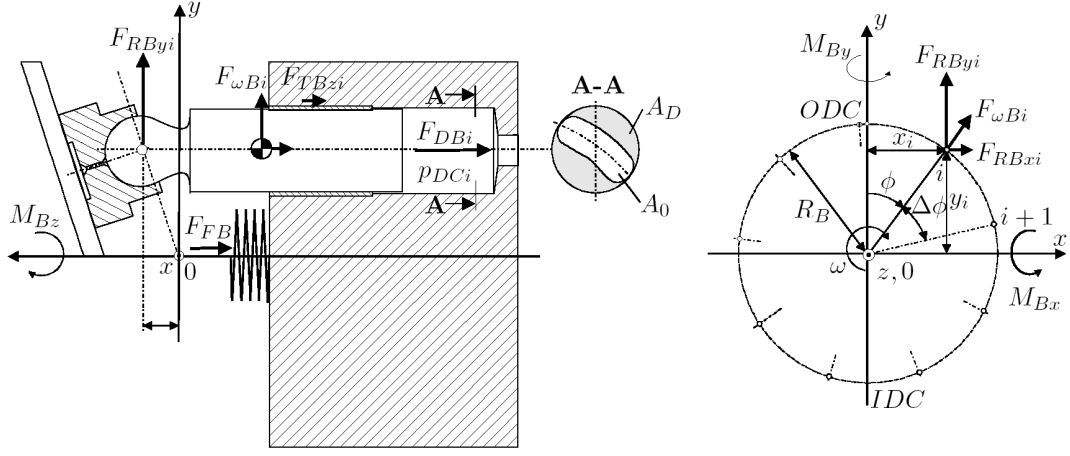$$F_{\omega Bi} = F_{\omega Ki} = m_K \omega^2 R_B \tag{2.47}$$

Figure 2.10: Forces acting at the cylinder block

The frictional force at the block is in the opposite direction of the frictional force of the pistons

$$F_{TBzi} = -F_{TKzi} \tag{2.48}$$

The cylinder block is also loaded with the frictional force from each slipper

$$F_{RBxi} = F_{\omega Ki} \sin\phi - F_{TGi} \cos\phi \tag{2.49}$$

$$F_{RByi} = F_{SKyi} + F_{\omega Ki} + F_{TGi} \sin\phi \tag{2.50}$$

The total external forces loaded at the cylinder block in each direction is

$$F_{Bx} = \sum_{i=1}^{n} F_{RBxi} \tag{2.51}$$

$$F_{By} = \sum_{i=1}^{n} F_{RByi} \tag{2.52}$$

$$F_{Bz} = F_{Ban} = -F_{FB} + \sum_{i=1}^{n} F_{DBi} + \sum_{i=1}^{n} F_{TBzi} \tag{2.53}$$

where n stand for the number of pistons. The F_{FB} force is transmitted due to a spring that is located between the cylinder block and swash plate. Its function is to prevent the gap between the cylinder block and valve plate to become to big, which would make the cylinder block to fly and the gap looses its function as a bearing. This would result in too large fluid forces.

The external moments around the x and y-axis are defined as

$$M_{Bx} = \sum_{i=1}^{n} y_i F_{DBi} + \sum_{i=1}^{n} y_i F_{TBzi} - \sum_{i=1}^{n} z_i F_{RByi} \tag{2.54}$$

$$M_{By} = -\sum_{i=1}^{n} x_i F_{DBi} - \sum_{i=1}^{n} x_i F_{TBzi} + \sum_{i=1}^{n} z_i F_{RBxi} \tag{2.55}$$

The corresponding fluid force and moments are described as

$$F_{fB} = \int_{A} p \, dA \tag{2.56}$$

$$M_{fBx} = \int\limits_{A} F_{fB} y \, dA \tag{2.57}$$

$$M_{fBy} = \int\limits_{A} -F_{fB} x \, dA \tag{2.58}$$

The fluid forces are balanced in the same way as for the slipper.

The fluid forces for all the interfaces are determined by solving the Reynolds and energy equation numerically for each gap, this is further explained in Section 3.2.

3 CASPAR

CASPAR (Calculation of Swash-Plate Type Axial Piston Pump/Motor) is a computational software that is designed to calculate the losses due to viscous friction and gap flow in swash plate type axial piston machines [2]. It also takes deformation due to pressure and thermal loading of solid parts into account.

CASPAR is divided into two parts, the *Pressure Module* and the *Gap Flow Module*. The *Pressure Module* calculates the pressure in the displacement chamber based on a lumped parameter model for the pressure. The *Gap Flow Module* solves the gap flows using the Reynolds, energy, and linear elastic deformation equation [2]. It uses the Finite Volume Method (FVM) to solve the for the fluid and the Finite Element Method (FEM) to solve for the solid parts.

When using *CASPAR*, the *Pressure Module* needs to be solved first. The complete calculated results from the *Pressure Module* are then used as a boundary condition in the *Gap Flow Module*.

The following sections will go through the theory of the *Pressure Module* and the *Gap Flow Module* that is relevant in order to understand how the program works.

3.1 Pressure Module

The *Pressure Module* uses a lumped parameter model for the pressure, which means that the pressure is assumed to be constant in the spatial domain. The model only regards changes with respect to time.

The following equation solves the pressure in the displacement chamber

$$\frac{dp_{DC}}{dt} = \frac{K}{V} \left(Q_r + Q_{SK} + Q_{SB} + Q_{SG} - \frac{dV}{dt} \right) \tag{3.1}$$

Equation 3.1 is the pressure equation, which is the main equation that is solved in the *Pressure Module*. K is the bulk modulus which depends on the temperature and pressure in the displacement chamber. The temperature is assumed to be constant in the ports. The displacement chamber is assumed to have the temperature of the fluid of the respective port that it is open to at an instant of time.

The pressure, p_{DC}, and the volume, V, are solved in time. The volume represents the displacement chamber volume.

The flow variable, Q_r, is the net flow through the valve plate

$$Q_r = Q_{rLP} + Q_{rHP} \tag{3.2}$$

where Q_{rLP} and Q_{rHP} is the sum of all the flows entering and exiting the displacement chambers for every piston. They are defined as in Equations 3.3 and 3.4
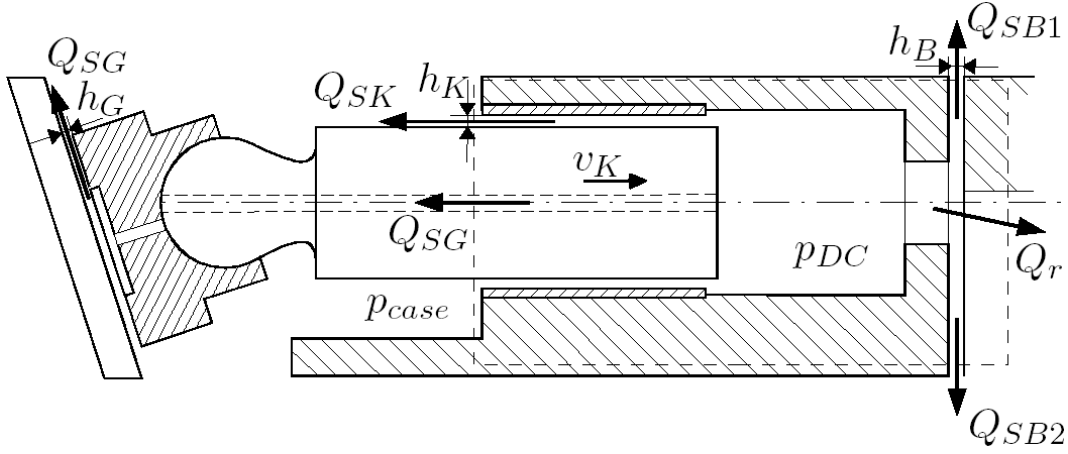
Figure 3.1: Pressure development in the displacement chamber

$$Q_{rLP} = \sum_{i=1}^{n} Q_{rLPi} = \alpha_{D,LP} A_{rLPi} \sqrt{\frac{2|p_{DCi} - p_{LP}|}{\rho}} sgn(p_{DCi} - p_{LP}) \tag{3.3}$$

$$Q_{rHP} = \sum_{i=1}^{n} Q_{rHPi} = \alpha_{D,HP} A_{rHPi} \sqrt{\frac{2|p_{DCi} - p_{HP}|}{\rho}} sgn(p_{DCi} - p_{HP}) \tag{3.4}$$

where α_D is the respective discharge coefficient that depends upon the metering-edge-geometry and the Reynold's number [3]. The areas A_{rLP} and A_{rHP} are defined as the respective cross sectional orifice area perpendicular to the flow direction through the valve plate. The pressures p_{LP} and p_{HP} is the pressure in respective port and n is the number of pistons.

The other flow variables in Equation 3.1 is Q_{SK}, Q_{SB}, Q_{SG}, which represents the leakage flows through the lubricating gaps between piston-cylinder, cylinder block-valve plate, and between slipper-swash plate respectively. The leakage in the cylinder block-valve plate interface, Q_{SB}, is the sum of Q_{SB1} and Q_{SB2}. The leakage flows is not calculated with the *Pressure Module* since this requires much information and knowledge of the gaps. Hence Q_{SK}, Q_{SB}, Q_{SG} are set to empirically determined values when first solved. This will be further described in the Section 3.2.

Equation 3.1 is modified in the following way to solve for the pressure in the HP and LP port.

$$\frac{dp_{LP}}{dt} = \frac{K}{V_{LP}} \left(Q_{IN} - Q_{rLP} \right) \tag{3.5}$$

$$\frac{dp_{HP}}{dt} = \frac{K}{V_{HP}} \left(Q_{rHP} - Q_{OUT} \right) \tag{3.6}$$

where Q_1 and Q_2 are the flows entering and exiting the LP and HP ports depending on the direction of flow.

$$Q_1 = \alpha_{D,LP} A_{D,LP} \sqrt{\frac{2|p_1 - p_{LP}|}{\rho}} sgn(p_1 - p_{LP}) \tag{3.7}$$

$$Q_2 = \alpha_{D,HP} A_{D,HP} \sqrt{\frac{2|p_2 - p_{HP}|}{\rho}} sgn(p_2 - p_{HP}) \tag{3.8}$$

The areas $A_{D,LP}$ and $A_{D,HP}$ are the areas in the throttling valves that is located at the entrance and exit to the pump. These areas regulate the amount of flow entering and exiting the pump, thereof the load of the system. The pressures p_1 and p_2 direct the line of flow in the system, a schematic of the axial piston pump and the connected lines can be seen in Figure 3.2.
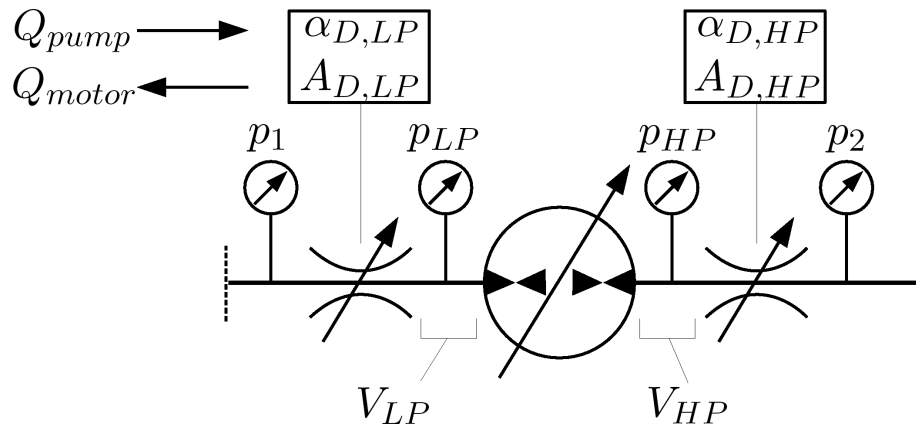

Figure 3.2: Schematic of the axial piston pump with the connected lines.

When the pump is in pumping mode, the pressure p_1 needs to be larger than p_2 in order for the flow to go in through $A_{D,LP}$ and out through $A_{D,HP}$. Pressure p_1 also needs to be equal to or larger than p_{LP}.

The same way follows for the pressure p_{HP} which needs to be larger than or equal to p_2, but smaller than p_{LP}. The areas $A_{D,LP}$ and $A_{D,HP}$ needs to be determined properly in order to full fill these pressure correlations to get the correct load on the system.

Figure 3.3 below shows how the pressure in the displacement chamber varies during one shaft revolution. The pressure profile is shown for pumping mode with the piston at the ODC for $\phi = 0°$.
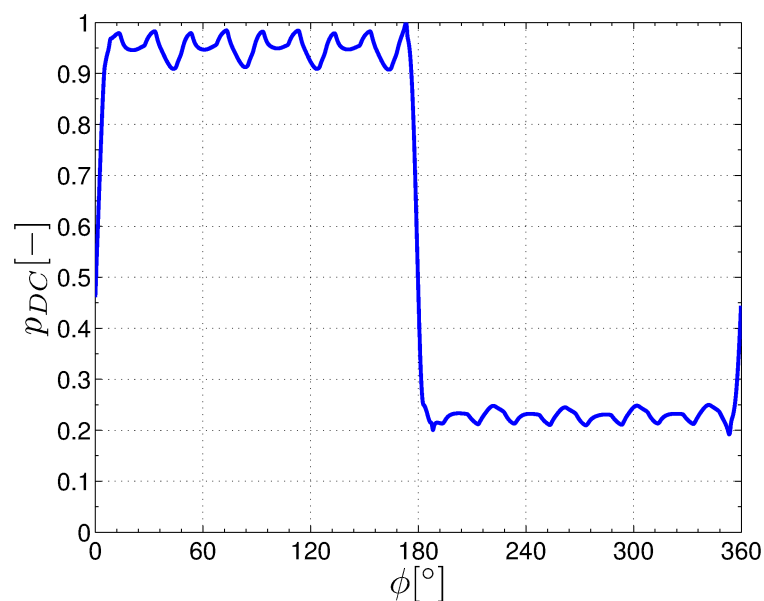

Figure 3.3: Pressure in the displacement chamber for a piston during one revolution. (Normalized with the maximum pressure)

The graph in Figure 3.3 is taken from a calculation of the original version of the *Pressure Module* that uses the equations 3.1-3.8.

The *Pressure Module* has several different versions that have been developed for different purposes, such as noise reduction in the pump. These versions can be viewed in Figure 3.4
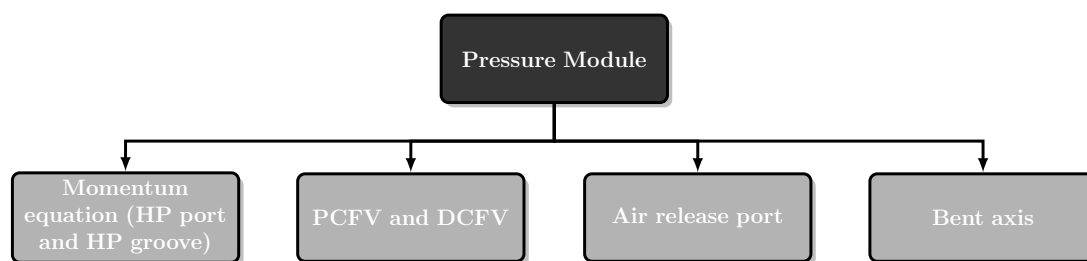

Figure 3.4: Existing versions of the *Pressure Module*

The different versions all originate from the original *Pressure Module* explained above. The following sections will go through the implementations already made in the different versions.

3.1.1 Momentum equation

The momentum equation was implemented in a model by Klop (2010), in order to investigate noise sources in hydraulic transmissions. One of the largest source of noise generation in an axial piston machine is the fluid borne noise. The fluid borne noise source can be quantified through the amplitudes of pulsating flow or pressure. The momentum equation was implemented in the HP port in order to more accurately capture these pressure amplitudes. The momentum equation was also implemented in the HP groove to capture pressure spikes that are shown by direct measurements of the displacement chamber pressure. This is since there is separation of flow which forms a jet in the instant when the piston is only open to the groove [1], see Figure 3.5.
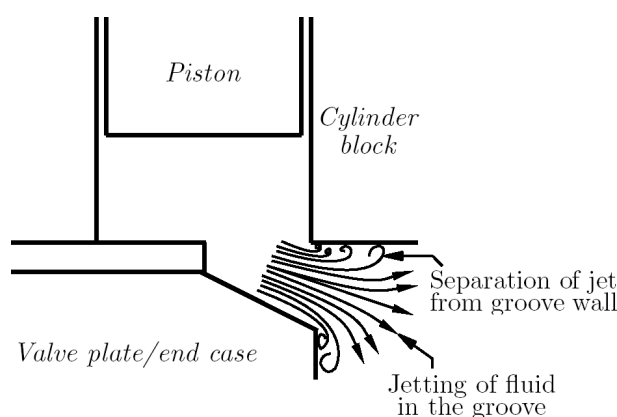
Figure 3.5: Flow through HP groove in a thick valve plate

The model also coupled the pump to a transmission line model in order to investigate new strategies to reduce noise [4]. The line model will not be used in the *Coupled Pressure Module* and is therefore not relevant to describe in this thesis. The line will instead be solved with a pressure equation in the same way as in the HP port as explained in the original *Pressure Module*.

The momentum equation was implemented in the HP port and HP groove. The implementation of the momentum equation in the HP port will capture the acceleration of fluid from the valve plate to the exit of the HP port. The momentum in the HP groove will capture the acceleration of fluid through the groove.

The following equation is implemented in the HP port

$$\frac{dv}{dt} = \frac{1}{V_{HP}\rho_{HP}}\left[\overrightarrow{F}_{FMIN} - \overrightarrow{F}_{FMOUT} + \overrightarrow{F}_{perm} + \overrightarrow{F}_{imperm}\right] - \frac{1}{\rho_{HP}}\frac{\frac{dp_{HP}}{dt}}{\frac{dp_{HP}}{d\rho_{HP}}}v \tag{3.9}$$

This is a differential equation of the velocity of flow exiting the HP port, and it is derived from the linear momentum equation. $\overrightarrow{F}_{FMIN}$ is the sum of the forces due to momentum of the fluid that is entering the HP port from the displacement chamber.

$$\overrightarrow{F}_{FMIN} = \sum_{i=1}^{n}\rho_i A_{rHPi}v_{rHPi}|v_{rHPi}| \tag{3.10}$$

where the incoming velocity to the HP port is, v_{rHPi}, which is determined by the following equation.

$$v_{rHPi} = \frac{Q_{rHPi}}{\alpha_{D,HP}A_{rHPi}sgn(p_{DCi} - p_{HP})} \tag{3.11}$$

Equation 3.11 is derived from Equation 3.4. The force of the fluid flow from HP port to the line is expressed as $\overrightarrow{F}_{FMOUT}$, which is calculated as

$$\overrightarrow{F}_{FMOUT} = \rho_{line}A_{line}v_{rHPi}|v_{rHPi}| \tag{3.12}$$

where A_{line} is the cross-sectional area of the line. The line is not visible in the equations for the original *Pressure Module* since the acceleration of the fluid through the HP port to the line is not taken into consideration. Hence the pressure will be the same in the HP port and line. The $\overrightarrow{F}_{perm}$ term is the force acting on permeable surfaces through the valve plate and end case and the last term, $\overrightarrow{F}_{imperm}$, are the remaining area that is impermeable of the end case at the entrance of the HP volume. In the exit of the volume the impermeable surface is estimated based on the average pressure between the line and port. The impermeable surface is considered as the remaining area between the entrance of the line, A_{line}, and end case, A_{rHP}.

$$\overrightarrow{F}_{perm} = \sum_{i=1}^{n}p_{DCi}A_{rHPi} - p_{line}A_{line} \tag{3.13}$$

$$\overrightarrow{F}_{imperm} = (A_{rHP} - A_{rHPzi})p_{HP} + (A_{line} - A_{rHP})\frac{p_{HP} + p_{line}}{2} \tag{3.14}$$

The opening areas through the end case can be viewed in Figure 3.6 and 3.7 respectively.

The pressure built up equation in the line is solved with Equation 3.15.

$$\frac{dp_{line}}{dt} = \frac{K}{V_{line}}(Q_{line} - Q_2) \tag{3.15}$$

where V_{line} and Q_{line} is the volume and the volumetric flow rate in the line. The volumetric flow rate is calculated with Equation 3.16.

$$Q_{line} = \alpha_{D\_Line}A_{line}v \tag{3.16}$$
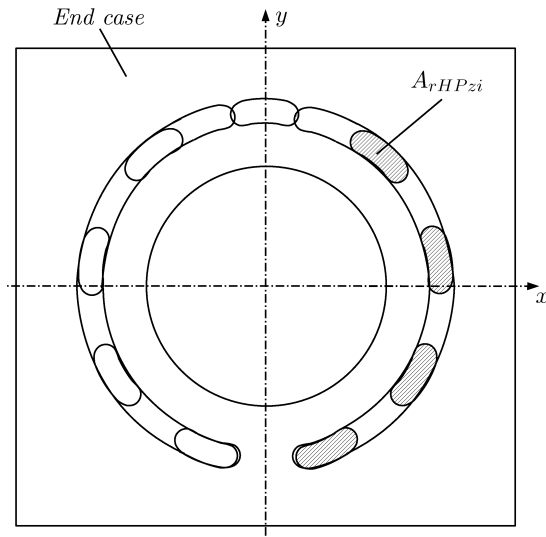
Figure 3.6: Cylinder block openings through the HP port
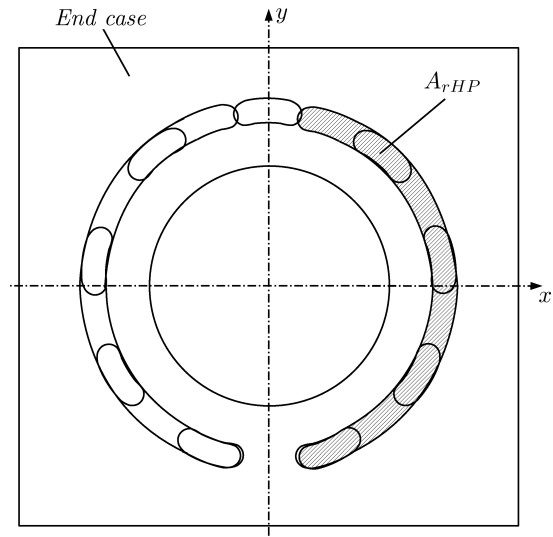
Figure 3.7: HP port opening

The pressure is solved in the line since the implementation of the momentum equation will change the pressure in the line compared to the HP port. A further description and a derivation of Equation 3.9 can be found in *Investigation of Hydraulic Transmission Noise Source* (Klop 2010).

The HP port, where Equation 3.9 is applied, can be viewed in Figure 3.8.
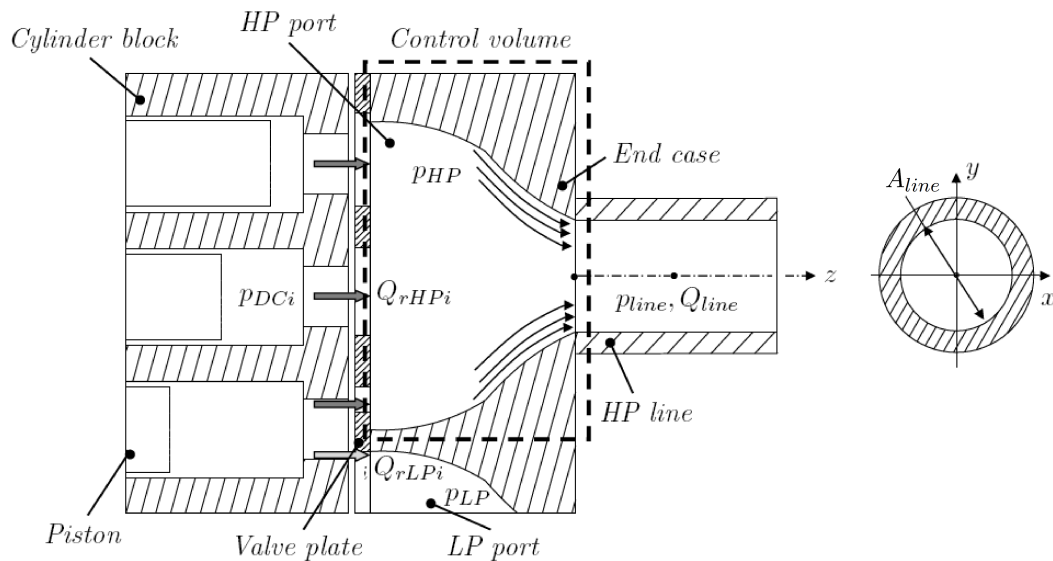
Figure 3.8: High pressure port control volume.

The momentum in the HP groove were implemented into the *Pressure Module* by Klop (2010). The momentum equation in the grooves is applied only when a cylinder opening are open to the HP groove. The angles ϕ_0 and ϕ_2 determines when this occurs, see Figure 3.9.

The momentum equation in the HP groove is used to derive the differential equation for the volumetric flow rate in the groove, which reads
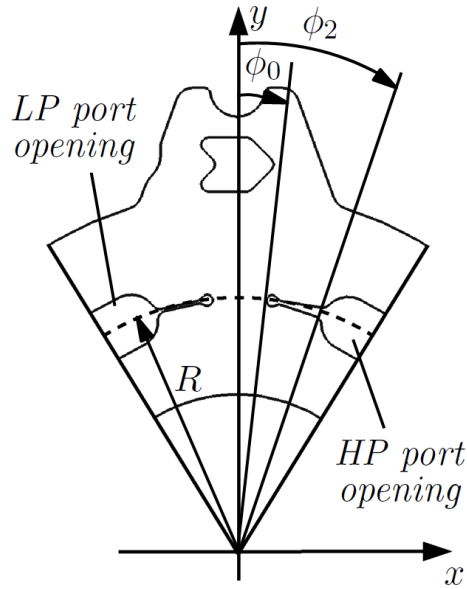
Figure 3.9: Starting and ending position over HP groove.

$$\frac{dQ_{gHP}}{dt} = \left(\frac{\Delta p}{\rho} - \frac{Q_{gHP}|Q_{gHP}|}{2A_{Hp}^2 \alpha_d^2} - \frac{1}{2}(v_2^2 - v_1^2) \right) \bigg/ \int_{\phi_0}^{\phi_2} \frac{R}{a} d\phi \qquad (3.17)$$

The first term in the nominator to the right side is associated with the total pressure drop between the displacement chamber and the HP port, the second term is the pressure drop from the displacement chamber to the smallest orifice. The third term is associated with the change in dynamic pressure drop over the length of the groove. The integration function in the denominator is changing with the location of the smallest orifice. A deeper look into the equation and its variables will be explained in Section 4.1.

Equation 3.17 were used to include the fluid mass effect into the HP groove for thin valve plates, see Figure 3.10

Figure 3.10: The mass of fluid accelerated through the HP groove in a thin valve plate ($\xi = 0$).

3.1.2 PC and DC filter volumes

The pre-compression and de-compression filter volumes (PCFV and DCFV) were implemented in order to prevent pressure spikes in the displacement chamber. These pressure spikes are a source of noise in the pump [2]. The filter volumes are placed in the end case, which are connected to the displacement chamber through small holes in the valve plate. The filter volu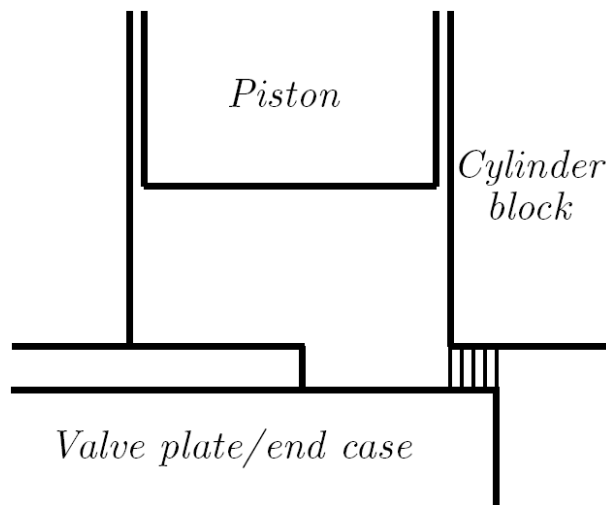mes have the same pressure as it is in the corresponding HP or LP port. The PCFV will help to pre-compress the displacement chamber before entering the HP port. The reversed will happen when it moves over the DCFV. The DCFV will then help the displacement chamber to decompress before it moves over the LP port. The general equation for the pressure in a filter volume is solved with the following pressure equation.

$$\frac{dp_{FV}}{dt} = -\frac{K}{V_{FV}}Q_{FV} \tag{3.18}$$

where Q_{FV} is the volumetric flow rate in and out from the filter volume. The location of the holes through the valve plate accessing the filter volume are determined by the angles from the ODC (Outer Dead Center), which can be seen in Figure 3.11. This means that the locations are determined by angle ϕ_{PC} and $\phi_{DC} + 180°$. The areas of the holes are A_{PC} and A_{DC}.
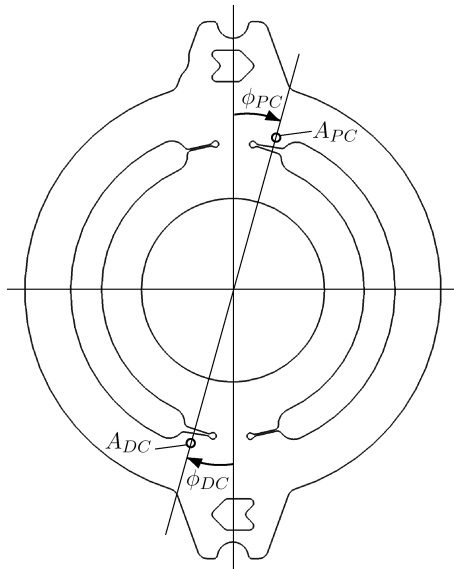
Figure 3.11: Location of the entry holes through the valve plate accessing PCFV and DCFV.

3.1.3 Air release port

The air release port is open directly to the case through a hole in the valve plate. It was implemented in order to reduce noise and the risk for cavitation [2]. When the piston is open to the air release port, high pressurized fluid that is left in the displacement chamber will be vented to the casing [2]. The pressure from the casing will depressurize the displacement chamber before the opening to the LP port. The air release port is placed next to the LP port, see Figure 3.12.

The pressure in the case, p_{case}, is constant and requires therefore not any equation for pressure. The flow exiting the displacement chamber into the case are defined as

$$Q_{AR} = \alpha_d A_{AR} \sqrt{\frac{2|p_{DC} - p_{case}|}{\rho}} sgn(p_{case} - p_{DC}) \tag{3.19}$$
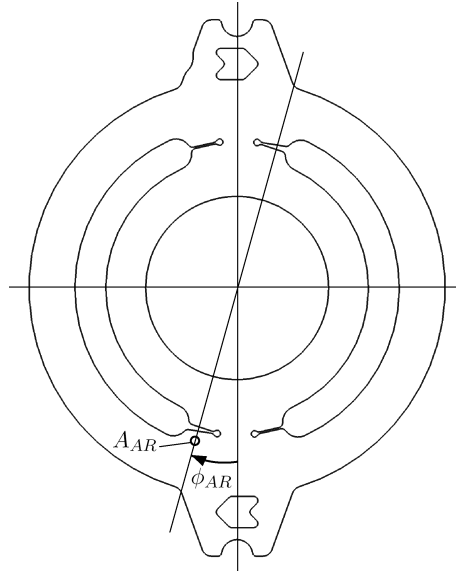
Figure 3.12: Location of the entry hole through the valve plate accessing the case.

3.1.4 Bent axis

CASPAR is made to simulate axial piston pumps of swash plate type design. The *Bent axis* model was implemented in the *Pressure Module* as a step towards a further development of *CASPAR* to be used for both designs.

The stroke is based on the pitch radius to the driving flange, R_D, instead of the pitch radius to the cylinder block, R_B, see Figure 2.3. The stroke length is therefore redefined as

$$s_K = -R_D \sin \beta (1 - \cos \phi) \tag{3.20}$$

The kinetics of the bent axis pump design are similar as for the swash plate design, hence the same relations can be used. The relative velocity of the piston is then

$$v_K = \frac{ds_K}{dt} = \frac{ds_K}{d\phi}\frac{d\phi}{dt} = \frac{ds_K}{d\phi}\omega = -\omega R_D \sin \beta \sin \phi \tag{3.21}$$

The volume entrapped in the displacement chamber is

$$V_{DC} = V_0 - s_K A_K = V_0 + R_D \sin \beta (1 - \cos \phi) A_K \tag{3.22}$$

The change of volume over time can then be expressed as

$$\frac{dV_{DC}}{dt} = v_K A_K = -\omega R_2 \sin \beta \sin \phi \tag{3.23}$$

3.2 Gap Flow Module

The *Gap Flow Module* is used in order to calculate the leakage flow rates Q_{SK}, Q_{SB}, Q_{SG} through the gaps, external forces, fluid forces and deformation due to pressure and thermal loading of solid parts. The gaps are solved independent from each other with a separate program for each gap. The Piston/Cylinder (P/C) gap is first solved independently from the other gaps. With results from the P/C program, the Slipper/Swash plate (S/Sp) gap can be solved. The last interface can be solved for the Cylinder block/Valve plate (Cb/Vp) by using the data calculated by the P/C and S/Sp, see Figure 3.13.
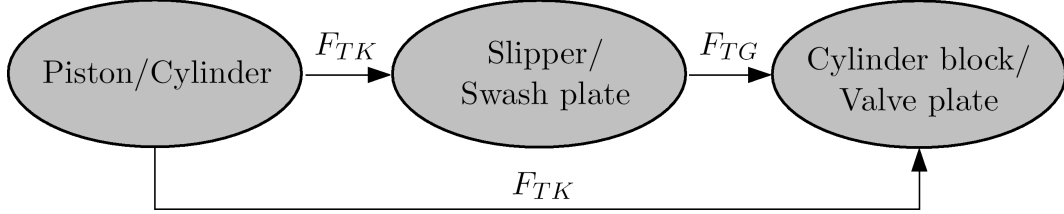
Figure 3.13: Forces transmitted in the *Gap Flow Module*.

The leakages is defined as the area integral of the velocity of flow leaking out to the case. The leakage for a piston is defined as

$$Q_{SKi}(\phi) = \int_0^{\pi d_K} \int_0^{h_K} u_y \, dz dx \tag{3.24}$$

Each piston has a different amount of leakage at a frozen instant of time. Hence all pistons should be summed for each angle of ϕ, hence

$$Q_{SK}(\phi) = \sum_i^n Q_{SKi}(\phi + i\Delta\phi) \tag{3.25}$$

where $\Delta\phi$ is the angle between each piston. The leakage for a slipper is defined in a similar way

$$Q_{SGi}(\phi) = \int_0^{2\pi} \int_0^{h_G} u_r a \, dz d\gamma \quad for \, a = a_2 \tag{3.26}$$

where each slipper needs to be summed, the same as for the piston

$$Q_{SG}(\phi) = \sum_i^n Q_{SGi}(\phi + i\Delta\phi) \tag{3.27}$$

The leakage for the block is different since it leaks out in two directions, both to the case inwards and outwards. The inward and outward leakage is denoted as Q_{SB1} and Q_{SB2}, respectively.

$$Q_{SB1} = \int_0^{2\pi} \int_0^{h_B} u_r r \, dz d\phi \quad for \, r = r_4 \tag{3.28}$$

$$Q_{SB2} = \int_0^{2\pi} \int_0^{h_B} -u_r r \, dz d\phi \quad for \, r = r_1 \tag{3.29}$$

The total leakage is the sum

$$Q_{SB} = Q_{SB1} + Q_{SB2} \tag{3.30}$$

As seen in Equations 3.24- 3.30 the leakage flow depends on the respective gap height, h_K, h_G, h_B. The gap height is varying in time and is non-constant along the gap, and it is therefore solved with the Reynolds equation (Equation 3.31). The Reynolds equation is derived from the Navier-Stokes and Continuity equations. It is derived based on assumptions that are valid in hydrodynamic lubrication. The fluid inertia forces are neglected, i.e. only viscous and pressure forces are considered. The pressure is assumed to be uniform along the gap height and the gradients of the velocity in the gap height direction are orders of magnitude larger than the gradients in the other directions. The fluid is also considered to be incompressible in the gaps.

$$
\begin{aligned}
&-\frac{\partial}{\partial x}\left(\frac{h^3}{12\mu}\frac{\partial p}{\partial x}\right) - \frac{\partial}{\partial y}\left(\frac{h^3}{12\mu}\frac{\partial p}{\partial y}\right) + h\frac{\partial}{\partial x}\left(\frac{(u_t + u_b)}{2}\right) + h\frac{\partial}{\partial y}\left(\frac{(v_t + v_b)}{2}\right) + \\
&+ \frac{(u_t + u_b)}{2}\frac{\partial h}{\partial x} + \frac{(v_t + v_b)}{2}\frac{\partial h}{\partial y} - \left(u_t\frac{\partial h_t}{\partial x} + v_t\frac{\partial h_t}{\partial y}\right) + \\
&+ \left(u_b\frac{\partial h_b}{\partial x} + v_b\frac{\partial h_b}{\partial y}\right) + (w_t - w_b) = 0
\end{aligned}
\tag{3.31}
$$

Index notation b and t stands for bottom and top surface and the velocities u, v abd w are in x, y and z direction which is along the gap length, width and normal. The gap height h is equal to $h_t - h_b$ which is the difference between the distance from the top to the reference plane and from the bottom surface to the reference plane, see Figure 3.14.
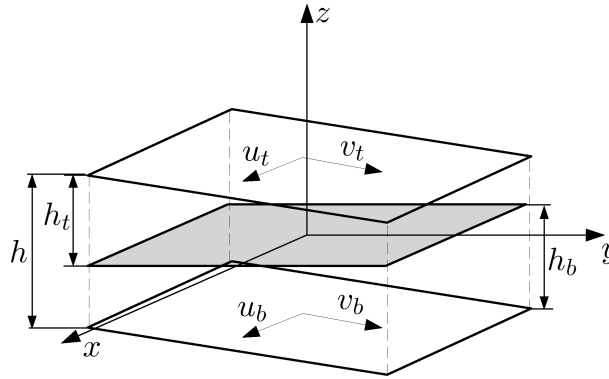
Figure 3.14: The reference plane in the lubricating gap. The reference plane is highlighted in gray.

The x- and y-axis are aligned with the reference plane, while the z-axis originates from the reference plane but is instead aligned in the direction of the gap height, hence h_b is defined as a negative value.

The first two terms in Equation 3.31 describe the net flow rates due to pressure gradients within the lubricating area; the third to sixth terms describe the net entraining flow rates due to the surface velocities. The seventh to ninth terms describes the net flow rate due to local expansion. The third and fourth term are the stretch terms that can be neglected. They are only of importance when the bounding solids are elastic [8].

The squeeze motion of the solid parts is represented by

$$\frac{\partial h}{\partial t} = w_t - w_b \tag{3.32}$$

Equation 3.31 can now be reduced to Equation 3.33.

$$-\frac{\partial}{\partial x}\left(\frac{h^3}{12\mu}\frac{\partial p}{\partial x}\right) - \frac{\partial}{\partial y}\left(\frac{h^3}{12\mu}\frac{\partial p}{\partial y}\right) + \frac{(u_t + u_b)}{2}\frac{\partial h}{\partial x} + \frac{(v_t + v_b)}{2}\frac{\partial h}{\partial y} +$$
$$- \left(u_t\frac{\partial h_t}{\partial x} + v_t\frac{\partial h_t}{\partial y}\right) + \left(u_b\frac{\partial h_b}{\partial x} + v_b\frac{\partial h_b}{\partial y}\right) + \frac{\partial h}{\partial t} = 0 \tag{3.33}$$

This equation is the main equation solved for each gap in *CASPAR*. The equation is however modified in each gap to solve the motions of the different parts. The velocities are determined by solving the N-S equations in the gaps.

The squeeze motion $\partial h/\partial t$ describes how the gap height is changing with respect to time and it describes the gap motions as a velocity of the moving parts. Figure 3.15 shows how the gap varies in the Cb/Vp interface.
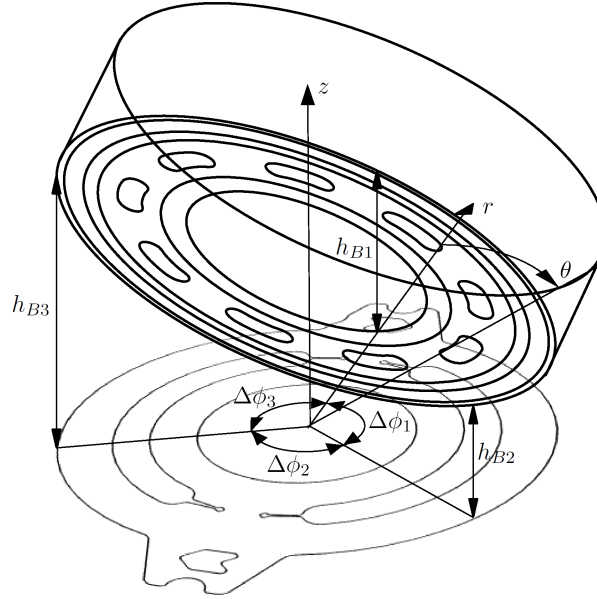
Figure 3.15: The varying gap between the cylinder block and valve plate

The tilting of the cylinder block can be described by the three points where the gap heights, h_{B1}, h_{B2}, h_{B3}, are acting. These gap heights are equidistant from each other, hence

$$\Delta\phi_1 = \Delta\phi_2 = \Delta\phi_3 \tag{3.34}$$

The total squeeze motion of the gap is described in these three points as $\partial h_{B1}/\partial t$, $\partial h_{B2}/\partial t$, $\partial h_{B3}/\partial t$. These three gap velocities are determined by the force balance between the external and fluid forces in the gap. The external forces and moments for the cylinder block (explained in Section 2.5) are transferred to act in these points. The transferred external forces and moments are denoted as, F_{e1}, F_{e2}, F_{e3} and the corresponding transferred fluid forces are denoted as , F_{f1}, F_{f2}, F_{f3}, see Figure 3.16. The force balance equations can then expressed as

$$\delta F_1 = F_{e1} - F_{f1}$$
$$\delta F_2 = F_{e2} - F_{f2} \tag{3.35}$$
$$\delta F_3 = F_{e3} - F_{f3}$$
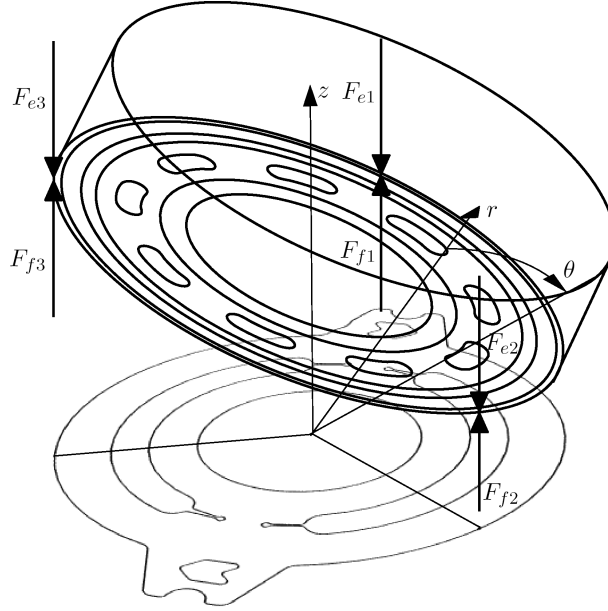
Figure 3.16: The external and fluid forces acting on the cylinder block.

At the beginning of each iteration these force balances are likely to be non-zero. The balance equation is treated as

$$|\delta F| = \sqrt{\delta F_1^2 + \delta F_2^2 + \delta F_3^2} \qquad (3.36)$$

If $|\delta F|$ is larger than the error criteria, the squeeze term in the Reynolds equation change hence the pressure in the gap will change. The squeeze term is changed according to a root finding method called Newton's method, which is not explained in this thesis. The correct gap geometry is achieved when the force balance is below the error criteria, i.e close to zero.

The fluid flow is considered to be non-isothermal in the gaps. Reynolds equation is affected by the viscosity which is depending on the pressure and temperature in the lubricant in the following way

$$\mu = \mu_0 e^{\alpha_p p - k_T (T - T_0)} \qquad (3.37)$$

The energy equation is expressed with the same assumptions as for the derivation of the Reynolds equation where convection and diffusion are considered

$$\rho c_p \left(u_x \frac{\partial T}{\partial x} + u_y \frac{\partial T}{\partial y} \right) = \frac{\partial}{\partial x} \left(k \frac{\partial T}{\partial x} \right) + \frac{\partial}{\partial y} \left(k \frac{\partial T}{\partial y} \right) + \frac{\partial}{\partial z} \left(k \frac{\partial T}{\partial z} \right) + \mu \Phi_D \qquad (3.38)$$

The viscous dissipation term $\mu \Phi_D$ describes the amount of energy transferred to heat in the gaps. Considering a laminar flow and a Newtonian fluid, the viscous dissipation term is expressed as

$$
\begin{aligned}
\mu \Phi_D = {} & \mu \left(\frac{\partial u_x}{\partial y} + \frac{\partial u_y}{\partial x} \right)^2 + \mu \left(\frac{\partial u_y}{\partial z} + \frac{\partial u_z}{\partial y} \right)^2 + \mu \left(\frac{\partial u_z}{\partial x} + \frac{\partial u_x}{\partial z} \right)^2 + \\
& + 2\mu \left[\left(\frac{\partial u_x}{\partial x} \right)^2 + \left(\frac{\partial u_y}{\partial y} \right)^2 + \left(\frac{\partial u_z}{\partial z} \right)^2 \right] - \mu \frac{2}{3} \left[\frac{\partial u_x}{\partial x} + \frac{\partial u_y}{\partial y} + \frac{\partial u_z}{\partial z} \right]^2
\end{aligned} \qquad (3.39)
$$

The formulation in cylindrical polar coordinates reads

$$\mu\Phi_D = \mu\left(r\frac{\partial}{\partial r}\left(\frac{u_\theta}{r}\right) + \frac{1}{r}\frac{\partial u_r}{\partial\theta}\right)^2 + \mu\left(\frac{1}{r}\frac{\partial u_z}{\partial\theta} + \frac{\partial u_\theta}{\partial z}\right)^2 + \mu\left(\frac{\partial u_z}{\partial r} + \frac{\partial u_r}{\partial z}\right)^2 +$$

$$+ 2\mu\left[\left(\frac{\partial u_r}{\partial r}\right)^2 + \left(\frac{1}{r}\frac{\partial u_\theta}{\partial\theta} + \frac{u_r}{r}\right)^2 + \left(\frac{\partial u_z}{\partial z}\right)^2\right] - \mu\frac{2}{3}\left[\frac{1}{r}\frac{\partial(ru_r)}{\partial r} + \frac{1}{r}\frac{\partial u_\theta}{\partial\theta} + \frac{\partial u_z}{\partial z}\right]^2 \quad (3.40)$$

The temperatures in the displacement chamber, HP port, LP port and the temperature in the case are considered to be known, and is used as boundary conditions to solve the energy equation in the gaps.

The *Gap Flow Module* also provides an option to consider structural deformation and thermal effects of the solid parts in the interfaces. The temperature and pressure fields contribute as an external load at the solids causing elastic deformation of the structure [5]. A flow chart of the numerical procedure in the *Gap Flow Module* is presented in Figure 3.17

1. The initial values and boundary conditions are set.

2. The temperature distribution in the solid parts is calculated.

3. The thermal distribution is then used as a load to calculate the impact of the thermal effects on the deformation of the solid parts. The deformation is calculated with linear elastic deformation equations.

4. The deformation will change the gap height in the interface between the solid parts.

5. The deformation is calculated again by using the pressure distribution around the solid part.

6. The pressure and temperature distribution in the fluid film are then calculated with Reynolds and energy equation.

7. The thermal conductive heat fluxes is calculated in order to get the amount of energy that is going into the solid parts.

8. The gap height is calculated from the force balance obtained when comparing external and fluid forces. The squeeze motion is changed until the forces are balanced.

   The described procedure from the calculated gap height due to the deformation is repeated for every time step in the current revolution. When a new revolution is initiated, the temperature distribution in the solid parts are calculated. The convergence is achieved when the temperature distribution in the solid parts has converged.
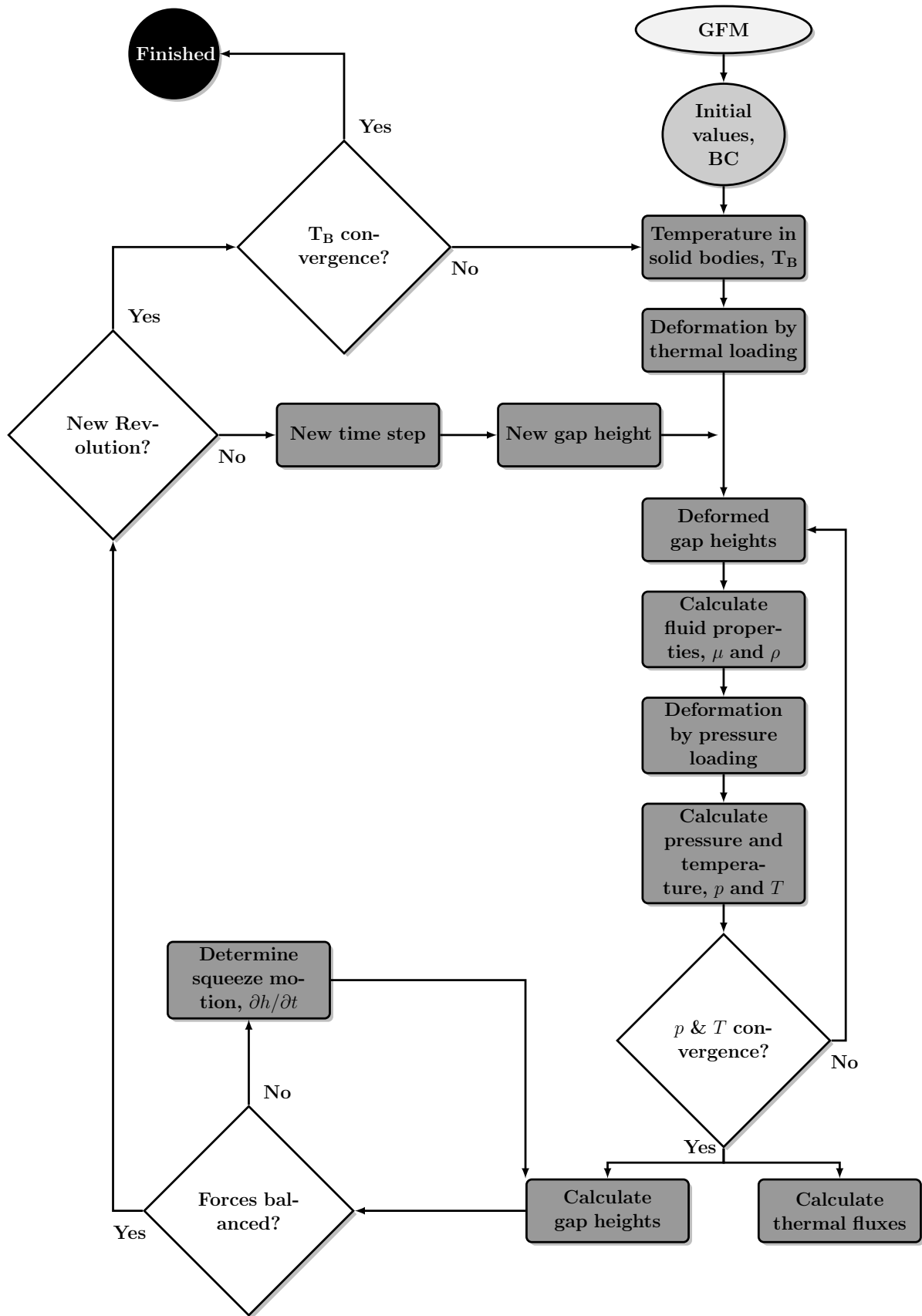
Figure 3.17: Flow chart of simulation procedure for the *Gap Flow Module*

4   Coupled Pressure Module

The *Coupled Pressure Module* contains all the functions that were previously separated in old versions of the *Pressure Module*, see Figure 4.1.
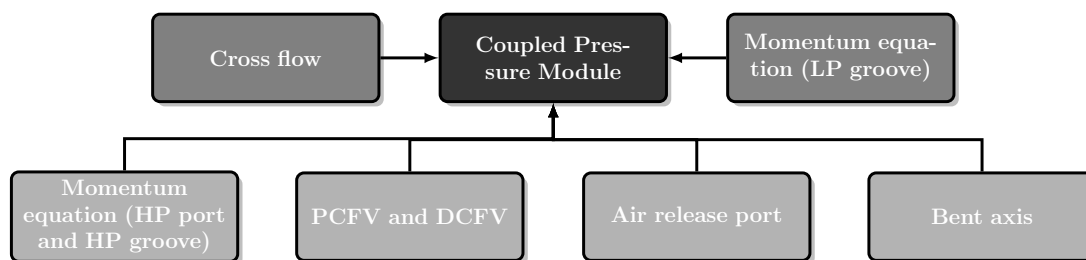

Figure 4.1: Versions of the *Pressure Module* and the new features that is integrated into the *Coupled Pressure Module*

The different versions are now in one single version. The benefits of this is that they can be combined together. There is also some new implementations in the *Coupled Pressure Module*.

The *Coupled Pressure Module* has the ability to:

1. Combine all previous versions together

2. Use the momentum equation in the groove for valve plates of thick designs

3. Use the momentum equation in the LP groove

4. Calculate the amount of cross flow

The following sections will describe how these new abilities have been implemented.

4.1   Momentum equation in groove

The momentum equation is implemented in the LP groove in order to capture the sudden dip in pressure when the piston is open to the groove.

The momentum equation in the HP groove was implemented by only considering thin valve plates where $\xi = 0$. This has been modified in the *Coupled Pressure Module* in order to also cover thick valve plates where $\xi > 0$.

In order to use the momentum equation in the LP groove, the angular positions of the LP groove is determined in the same way as for the HP groove. The positions are described by ϕ_3 and ϕ_4, which are located at the beginning and at the end of the groove respectively, see Figure 4.2.

In order to understand how the momentum equation now also works for thick valve plates, a derivation of the differential volume flow rate equation for the HP groove is described. The differential equation for the LP groove is derived in a similar manner, hence it is not described.

The differential equation is derived by writing the momentum equation as the rate of change of momentum in a control volume of the groove for a thick vale plate with gradual opening ($\xi >> 0$), as in Figure 4.3a.

The derivation was made in *Cylinder pressure transients in oil hydraulic pumps with sliding plate valves* (Edge, K A., Darling, J 1986) with cartesian coordinates.
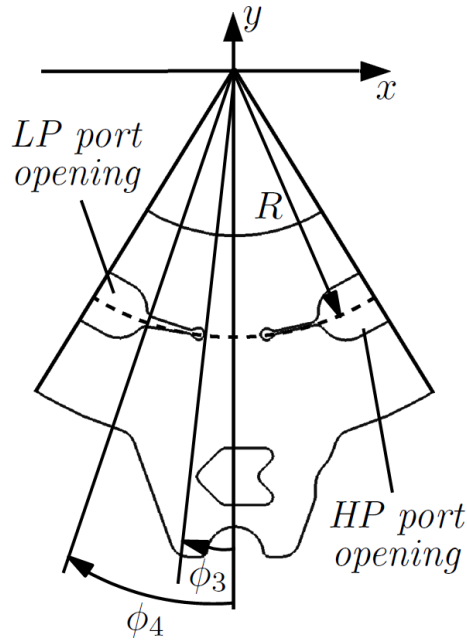
Figure 4.2: Starting and ending position over LP groove.

The derivation of Equation 4.7 begins with the momentum equation in cylindrical coordinates, Equation 4.1.

$$\frac{\partial p}{\partial \phi} a \delta \phi = m \left(\cos \xi \frac{v}{R_B} \frac{\partial v}{\partial \phi} + \frac{\partial v}{\partial t} \right) \tag{4.1}$$

where $\delta \phi << 1 \Rightarrow \sin \delta \phi \approx \delta \phi$.

The control volume covers the mass of fluid that is accelerated through the groove; this can be viewed in Figure 4.3, where a is the area of the control volume perpendicular to the flow direction. The velocities v_1 and v_2 are the entering and exiting velocity of the volume.

The pressure at point 1 is denoted P_1, which is acting on the area of the groove that is opened to the displacement chamber, A_{HP}. The pressure at point 2, P_2, is acting on the area opened to the HP port.
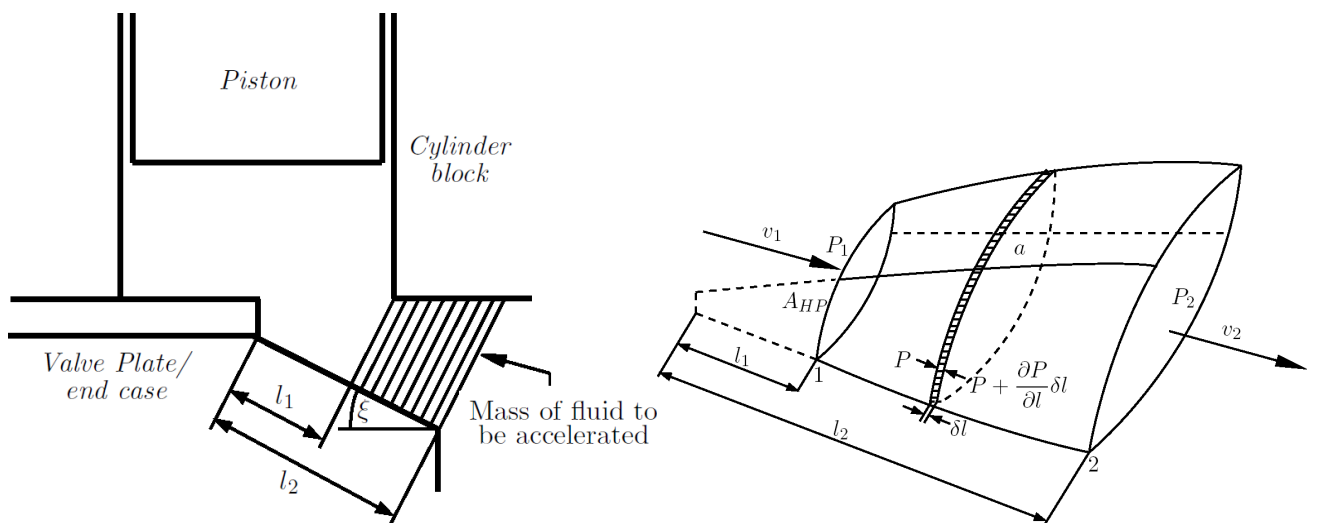
(a) The mass of fluid accelerated through the HP groove. (b) The volume of fluid accelerated through the groove, with the control volume represented as a slice, δl.

Figure 4.3: Fluid accelerated through HP groove

The radius R_B is the pitch radius of the cylinder block. The lengths l_1 and l_2 are equal to

$$l_1 = \frac{R_B \sin \phi_1}{\cos \xi} \tag{4.2}$$

$$l_2 = \frac{R_B \sin \phi_2}{\cos \xi} \tag{4.3}$$

The angle ϕ_1 are the current position of the cylinder opening. Equation 4.1 can be expressed in volumetric flow rate by substituting $m = \rho a R_B \delta \phi / \cos \xi$, $v = Q_{gHP}/a$ and $\partial v / \partial t = \partial (Q_{gHP}/a)/\partial t$, which will give Eq 4.4

$$\frac{\partial p}{\partial \phi} = \frac{\rho Q_{gHP}}{a} \frac{\partial v}{\partial \phi} + \frac{R}{\cos \xi} \frac{\rho}{a} \frac{\partial Q_{gHP}}{\partial t} \tag{4.4}$$

where Q_{gHP} is the volumetric flow rate of the flow through the control volume.
After assuming the fluid as incompressible and including the pressure drop due to the acceleration of the fluid through the groove

$$\Delta p_G = \rho \frac{\partial Q_{gHP}}{\partial t} \int_{\phi_0}^{\phi_2} \frac{1}{\cos \xi} \frac{R}{a} d\phi + \frac{\rho}{2}(v_2^2 - v_1^2) \tag{4.5}$$

and the pressure drop from the displacement chamber to the smallest orifice (vena contracta) [1]

$$\Delta p_0 = \frac{\rho Q_{gHP}|Q_{gHP}|}{2 A_{HP}^2 \alpha_d^2} \tag{4.6}$$

the differential equation for the volumetric flow rate through the groove into the HP port is derived as Equation 4.7.

$$\frac{dQ_{gHP}}{dt} = \left(\frac{\Delta p}{\rho} - \frac{Q_{gHP}|Q_{gHP}|}{2 A_{Hp}^2 \alpha_d^2} - \frac{1}{2}(v_2^2 - v_1^2) \right) \bigg/ \int_{\phi_0}^{\phi_2} \frac{1}{\cos \xi} \frac{R}{a} d\phi \tag{4.7}$$

The terms is explained in Section 3.1.1. A similar equation is used in the LP port, but with appropriate indices.

4.2 Cross-Flow

The cross flow is defined as the volumetric flow rate that is entering the LP port from the displacement chamber, Q_{CF}. This flow is assumed to be all the flow that is leaving the displacement chamber through the LP port, hence when Q_{LP} is negative. The amount of cross-flow is valuable when the efficiency of the pump is determined.

$$Q_{CF} = |Q_{LP} < 0| \tag{4.8}$$
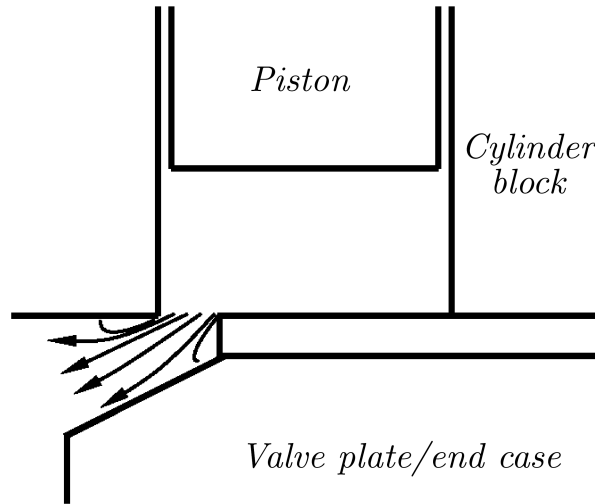
Figure 4.4: Flow entering the LP port.

5 Coupled Gap Flow Module

The *Gap Flow Module* (GFM) calculates each gap separately. This is both time-consuming and inefficient. Such a calculation method will be less accurate than simultaneous solution with exchange of simulation results after each iteration. This is since information is passed between the interfaces in order to calculate the flow field in the gaps correctly.

The CGFM is the "parent" program which controls the order and when a simulation for a leakage interface should start. When a simulation is called, a separate "child" process is created. Each simulation will have their own child process. The processes/simulations runs in parallel in order for each simulation to interact with each other. The simulations interacts by continuously reading output from the corresponding interface in order to get the appropriate information for each gap. The information that is transmitted between the simulations are friction forces created in the P/C and S/Sp interfaces.

5.1 Transmitting forces

CGFM solves the leakage flows simultaneously by exchanging friction forces with each other. The P/C interface transmits the friction force, F_{TK}, to the S/Sp interface. P/C interface also receives the frictional force, F_{TG} from the S/Sp interface. The Cb/Vp interface will receive the friction forces from both the P/C and S/Sp interfaces, this can be seen in Figure 5.1.

Figure 5.1: Passing of forces

The P/C interface is solved by calculating the flow field for one piston, because all pistons goes through the same cycle during a revolution. The same rule applies for the flow field in a S/Sp interface. Hence there is only one friction force transferred for each time-step between the P/C and S/Sp. The Cb/Sp interface is different, so this interface requires a friction force from all pistons and slippers for each time-step, in order to get the external force and moments acting on the cylinder block, as explained in Section 2.5.
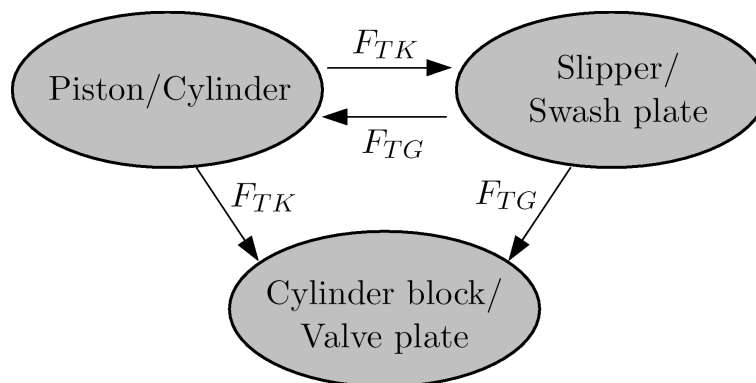
5.2 Implementations

To understand how the leakage interfaces interact programming wise, there are some implementations in the CGFM that need some further explanation.

5.2.1 Interpolation

The first thing that is checked when a force is received from another simulation is the angular step, $\Delta\phi$, which is the amount of degrees between two time-steps, $\Delta\phi$. If all simulations use the same angular step, there would in theory be no need for any interpolation, since the simulations would have the same corresponding time-steps. But since the CGFM program is programmed in C++, it uses the floating point number system.

The floating point number system will not be explained in this thesis, but what basically happens is that a decimal number, that for example should be 0.0004, instead can be represented as 0.000399999 or 0.000400001. This becomes a problem when two numbers are expected to be the same, like two time steps. A way that partially solves this is to introduce an interpolation method, and since the simulations should be able to run with each other with different angular steps, the introduction of the interpolation is necessary.

The simplest method is the first order linear interpolation method, since it only uses two points to approximate another point between those points. The two points will be called, end points, and the approximated point, interpolation point. The first order linear interpolation is safer than higher order methods, such as cubic interpolation, were the error can be more significant when large derivatives are encountered in the data, since it bases its interpolated value on more than two points.

$$\frac{F - F_i}{t - t_i} = \frac{F_{i+1} - F_i}{t_{i+1} - t_i} \tag{5.1}$$

The relation for the linear interpolation can be viewed Equation 5.1. F and t represents force and time respectively. The index notation $i+1$ and i indicates if the end points is located at a larger or smaller time step than the current time step, t, respectively. The variables without notations are located in the interpolation point. By solving for F in Equation 5.1, the force for the current time step is calculated.

The P/C and S/Sp only calculates forces for the first piston, which means that for each revolution it will begin to rotate from $0-360$ degrees. The simulation of the Cb/Vp interface on the other hand, calculates forces regarding each individual piston in the simulation, which means that the other pistons except the first will start to rotate from another angle depending on the number of pistons in the pump; this is illustrated in Figure 5.2 for a nine piston pump. The second piston will rotate from $40-40$ degrees and the other follows the same behavior from their initial angle. It is here important that the interpolation handles the shift from the last time step in a revolution to the first time step in the next revolution.

All pistons will be calculated based on the same values that were calculated in Piston/-Cylinder and Slipper/Swash plate simulations where all pistons are treated with the same behavior as the first piston.
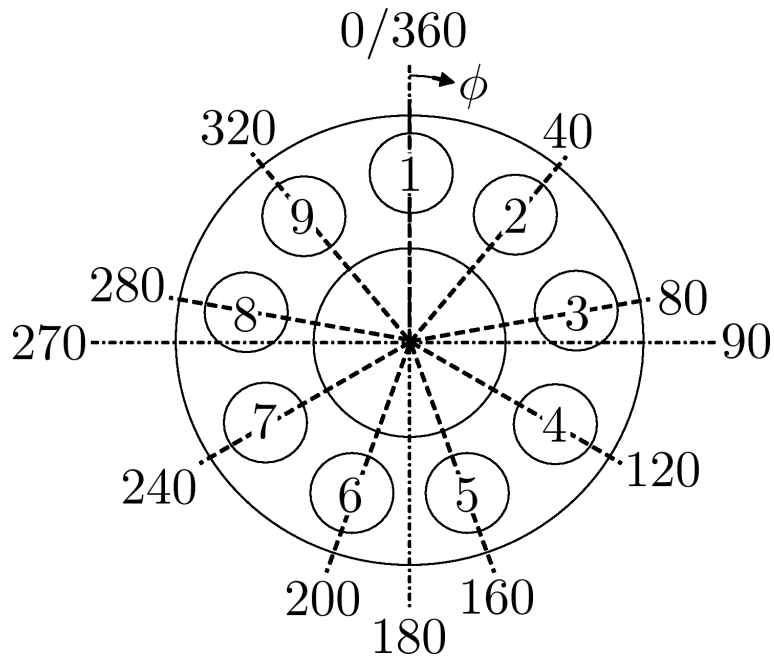
Figure 5.2: Cross-section of the cylinder block in an axial piston pump with nine pistons and their corresponding initial angles.

5.2.2 Offset

The offset is introduced to fix the floating point number system problem that is explained in Section 5.2.1. The offset will increase the tolerance in the end points where the interpolation point should lie within. The problem arises when an interpolation point should be located at an end point, but since the floating point problem exists it will instead be slightly smaller or larger. This is not really an issue if a rotating piston is somewhere between $0 - 360$ degrees of a revolution because of the implemented interpolation method. The interpolation only takes time-step values that correspond to angles between $0 - 360$ degrees; there will therefore be a floating point problem when a revolution that should take for example 0.04 seconds instead takes 0.040000001 seconds. The increased time will correspond to an angle larger than 360 degrees. As previously stated, increasing the end points interval will fix this.

   The offset is implemented in a way that will increase the tolerance of the end points by one order larger than the order of a time-step. This is important in order for the tolerance not to become too large and in that sense overlap into the next end point at another time-step. If a time-step is $\Delta t = 0.00005$ seconds and t_{i+1} is 0.04 seconds, then t_i and t_{i+2} is 0.03995 and 0.04005 seconds respectively. Let say that t, which is in the interpolation point, should be equal to t_{i+1} but instead is equal to 0.0400001. This will locate the interpolation point in the wrong revolution. The offset will increase the tolerance with a value that is larger than the floating point error. Since the time-step in this example is the in order of 10^{-5} the tolerance will be in the order of 10^{-6}. Which in a sense virtually increase the value of t_{i+1} to 0.040001; this is illustrated in Figure 5.3. The same happens for t_i but instead of an increased value, the value is decreased to 0.039949. This lets the location of the interpolation point to be between 0.039949 and 0.040001 instead of 0.03995 and 0.04.
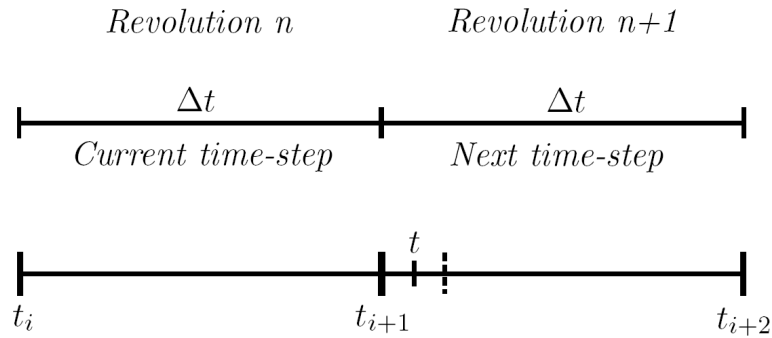
Figure 5.3: Illustration of the offset implementation (figure is not scaled).

5.2.3 Under-relaxation

Under-relaxation is implemented to avoid large discontinuities in the simulation that can make it diverge. A discontinuity can happen when a force is received from another simulation that is much larger/smaller than the estimated force in the current simulation. So the idea of under-relaxation is to take some part of the old value and the rest of the new value. This will give a force between the old and new force, which makes a smoother transition. Equation 5.2 shows how the new force, F, is calculated by the current simulation.

$$F = F^{n-1} + \alpha \left(F^n - F^{n-1} \right) \qquad n = 1, 2, 3... \tag{5.2}$$

Index $n - 1$ indicates that the force is from the previous revolution while the index n indicates that the force is from the current revolution. The under-relaxation factor, α, can vary between 0–1, where a value of 0 and 1 would only take the old and new force respectively. When the P/C and S/Sp begin their simulations, they will initiate their first revolution, $n = 1$. Since no old force, F^0, is available for the first revolution, the under-relaxation factor is recommended to be set to 1, in order to only use the new force, F^1.

5.3 Methodology of CGFM

CGFM program starts by calling the simulations of the P/C and the S/Sp. At the first revolution for each simulation, the interfaces will estimate the friction force from the corresponding interface, this is since none has completed their first revolution. Each simulation will check if the other simulation has completed a revolution for each time a new revolution of the current simulation has been initiated. If so, the most recent completed revolution will be used instead of estimating the friction force. In this way, if one simulation is faster than the other (which is likely), the slower simulation will receive a force from the other simulation, while the faster simulation will continue to estimate the force at least throughout the second revolution.

The third simulation, Cb/Vp, starts when both the P/C and S/Sp has completed their first revolution; the same methodology is applied for this simulation as for the simulations of the P/C and S/Sp. The only difference is that Cb/Vp has to receive forces for every piston instead of just one, as for the other two simulations. The flow chart in Figure 5.4 gives a representation of the global simulation procedure in CGFM.
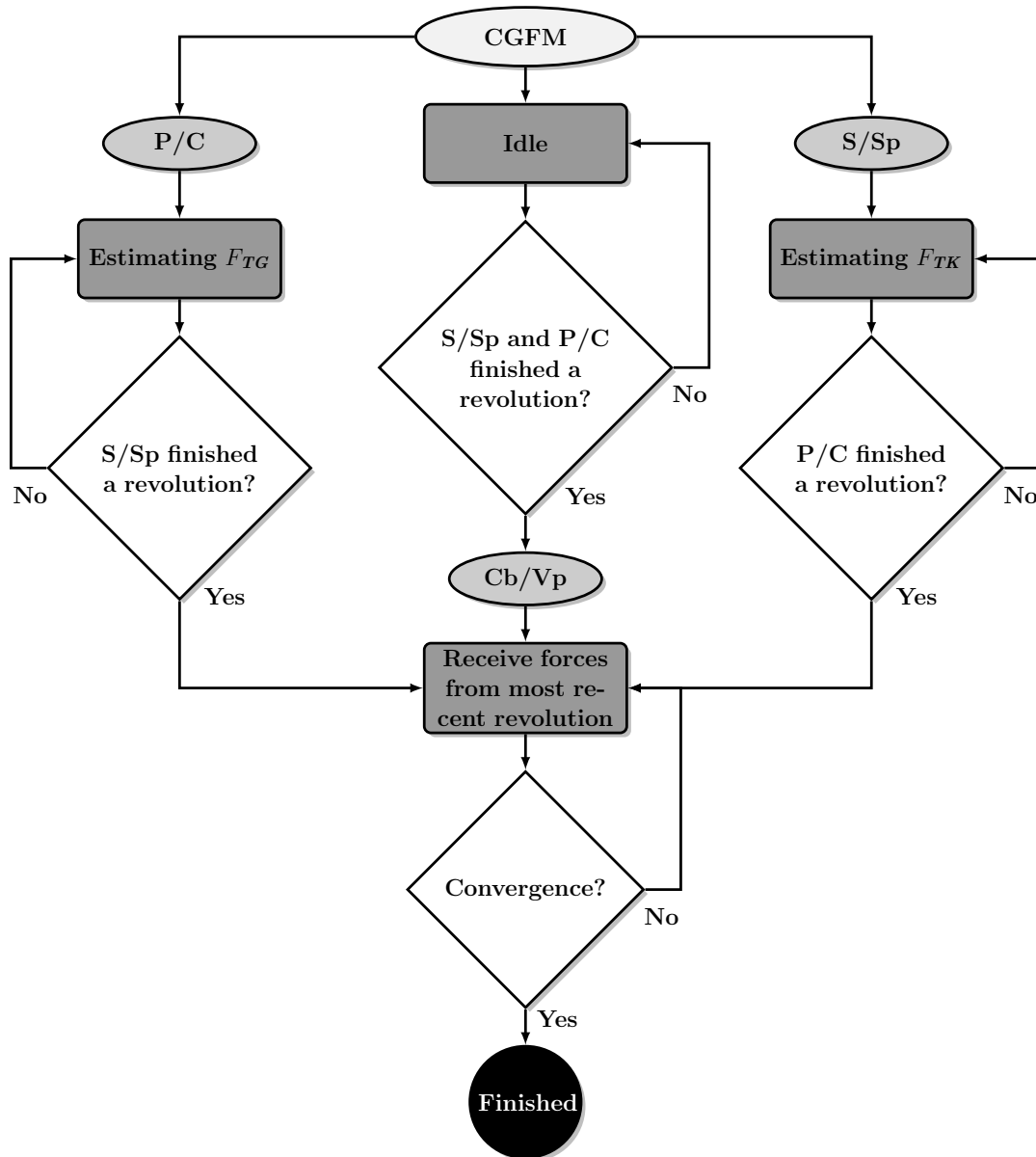
Figure 5.4: Flow chart of global simulation procedure in the *Coupled Gap Flow Module*

5.4 Validation

The figures in this section shows how the forces are treated for the respective simulation. The results below were simulated for the Sauer-Danfoss 75cc pump for 15 revolutions with a shaft speed of 3000 rpm and with maximum displacement ($\beta = 17°$). The under-relaxation factor was set to 0.5.

It can be seen in Figure 5.5 and Figure 5.6 that the S/Sp simulation completed its first revolution faster than the P/C simulation. This is since the shape of the P/C curve in the second revolution has been influenced by the values from S/Sp simulations first revolution, in Figure 5.6. The estimated F_{TK} force by the S/Sp is far from the correct force calculated by the P/C, see Figure 5.5.

As seen in Figure 5.7, the calculated force, F_{TK}, for the P/C simulation has almost converged after just a few revolutions. There is a visible maximum in the F_{TK} force for the P/C in revolution 2 and 8 that is not visible in the received force in the Cb/Vp. The calculated force, F_{TG}, for the S/Sp simulation does not reach convergence as fast as the

P/C simulation.

Figure 5.5: The force, F_{TK}, is calculated by the P/C simulation and transmitted to the S/Sp simulation.

Figure 5.6: The force, F_{TG}, is calculated by the S/Sp simulation and transmitted to the P/C simulation.

The F_{TG} force for the Cb/Vp in Figure 5.8 has not received a converged force from the S/Sp at the first revolution. It can clearly be seen in this figure, that the S/Sp simulation only has done one complete revolution, before the Cb/Vp simulation was initiated.

The trend is the same for all simulations, the new forces converges with the receiving forces. The under-relaxation prevents the receiving simulation from diverge by avoid discontinuities in the forces, as showed in Figure 5.6. Faster convergence can be achieved if the under-relaxation factor is increased from 0.5, but this is at the cost of the stability of the simulations.
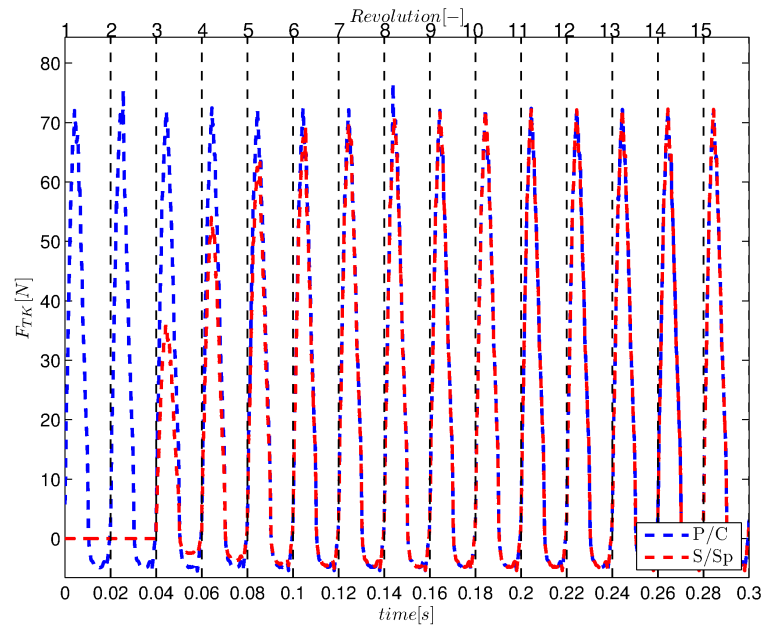
Figure 5.7: The force, F_{TK}, is calculated by the P/C simulation and transmitted to the Cb/Vp simulation.

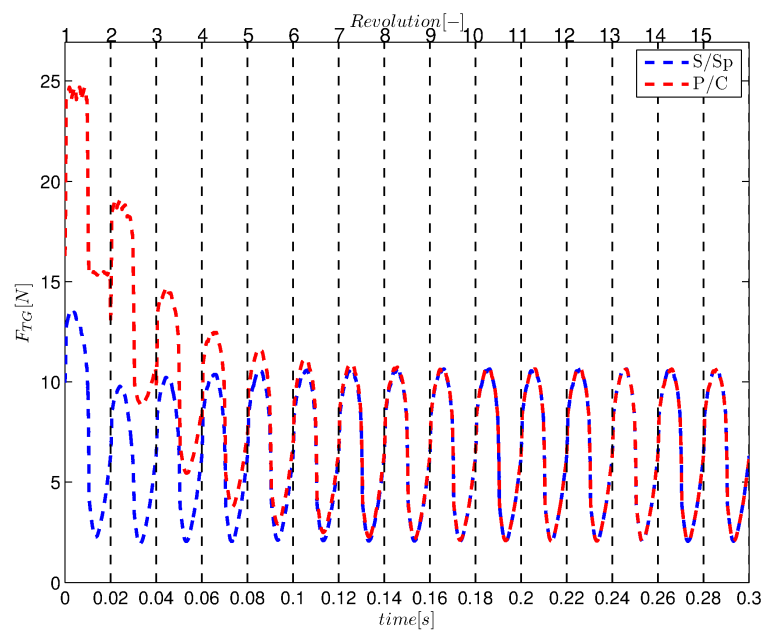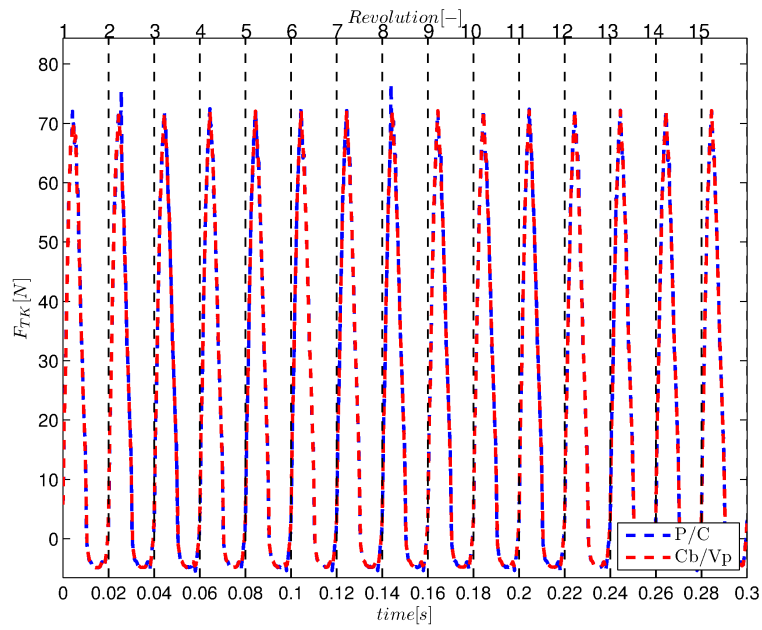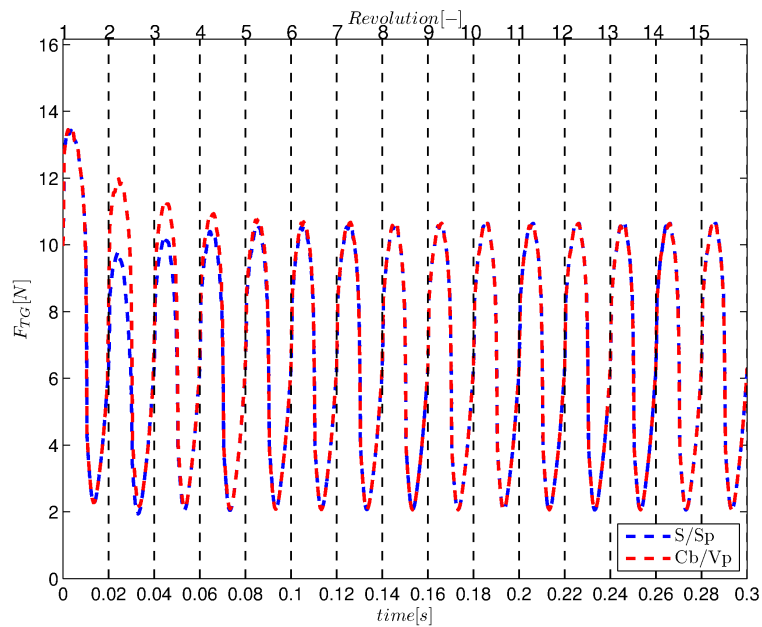Figure 5.8: The force, F_{TG}, is calculated by the S/Sp simulation and transmitted to the Cb/Vp simulation

6 Case temperature

The case temperature is the temperature in the pump case, see Figure 6.1. The case containing the pump is filled with oil that is lubricating the pump. The leakage from the lubricating gaps are flowing into the case, which is drained using the pump drain/case port. The temperature of the fluid in the pump case is elevated because of the energy dissipated in the gaps. It is also due to other losses occurring during pump operation like friction in shaft bearings and churning losses caused by rotation of the cylinder block in the oil filled case. The temperature of the fluid in the pump case is constant when the pump runs under steady state conditions where the ambient temperature is constant.
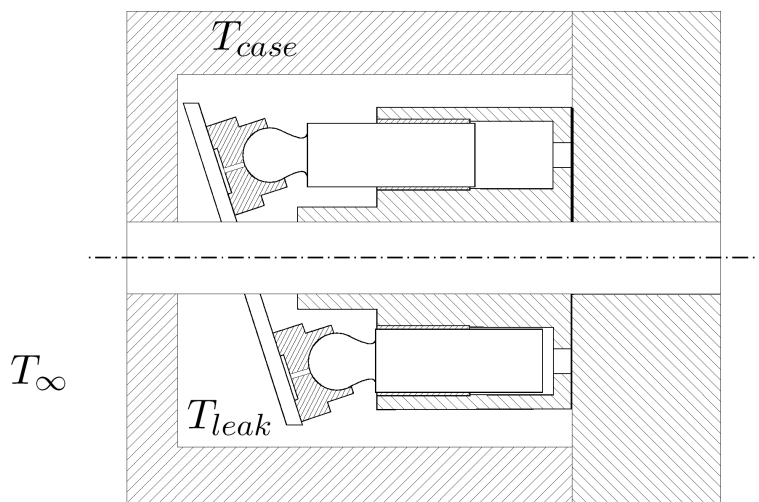
Figure 6.1: The pump case surrounding the rotating group of the pump.

The case temperature is a boundary condition in the *Gap Flow Module* in *CASPAR* in order to solve the energy equation and the structural deformation due to thermal loads. This temperature is not calculated in *CASPAR*, instead it is pre-defined based on measurements.

The model is developed in order to calculate the case temperature by using the viscous dissipation created in the three lubricating gaps. The energy dissipation due to rotation of cylinder block in the oil filled case will also be considered. The model is solved analytically hence only constant gap heights are assumed. The calculated temperature will then be validated against measured leakage temperatures that also were performed.

6.1 Measure the leakage temperature

The measurements were performed since there were no good data regarding the leakage temperature. The test rig was used with a *Sauer-Danfoss 75cc* axial piston machine, see Figure 6.2.

The electric motor(6) drives the shaft(5) that is connected to driving the pump. The inlet(2) provides the flow to the pump. Line (11) is the supply line to a charge pump which is providing pressure to a proportional valve that in turn is connected to the swash plate control piston, that is controlling the displacement of the swash plate. Without a charge pump the swash plate would not be able to be displaced. The charge pump adds power loss to the system and in order to reduce this loss, a line for the control pressure(10) is added to reduce the torque loss by maintaining pressure over the charge pump.
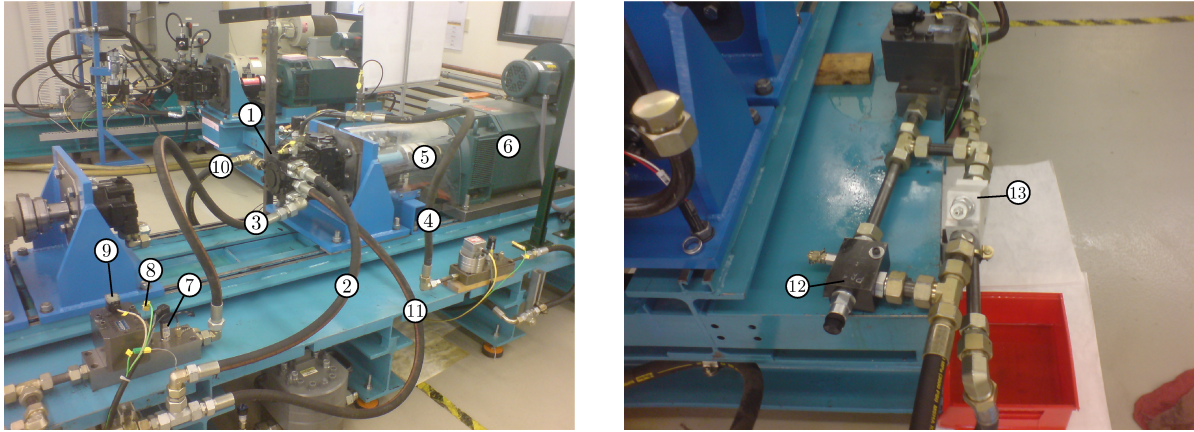
Figure 6.2: Sauer-Danfoss 75cc pump mounted on test rig. (1) Sauer-Danfoss 75cc pump, (2) LP line (inlet), (3) HP line (outlet), (4) Leakage line, (5) Shaft, (6) Electric motor, (7) Pressure sensor, (8) Thermo couple, (9) Flow meter, (10) Control pressure, (11) Charge pump line, (12) Adjustable throttling valve, (13) Pressure relief valve.

The pressure in the HP port can be controlled by the adjustable throttling valve(12) located along the HP line(3). The leakage will pass through line (4). The pressure relief valve(13) is there as a safety valve if the adjustable valve would be damaged. This valve will open at a certain pressure that should be above the maximum pressure used in the measurements.
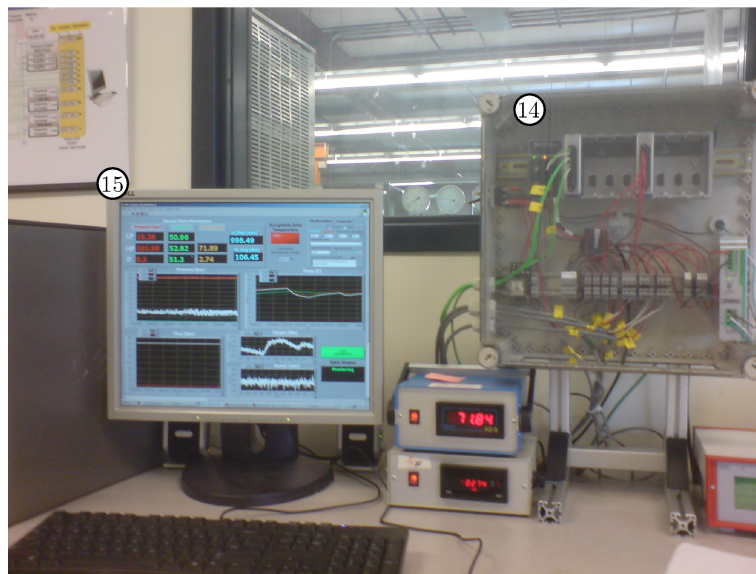
Figure 6.3: Control table. (14) Data Acquisition, (15) PC with LabVIEW.

The thermo couples(8), pressure sensors(7) and flow meters(9) were placed along the HP-, LP- and leakage line. The couples, sensors and meters are connected to the *DAQ* (Data Acquisition)(14) system where the analog signals are converted to digital and then read into the computer that uses *LabVIEW*, see Figure 6.3. The data screen(15) in *LabVIEW*, displays the pressure, temperature, flow rate, pump speed and the provided moment.

To provide the testing pump with the flow of oil, other pumps(16) are used to pump the flow in the system, see Figure 6.4. It is very important to provide the tested pump with enough flow to avoid cavitation. The flow that is needed to provide the pump is calculated by
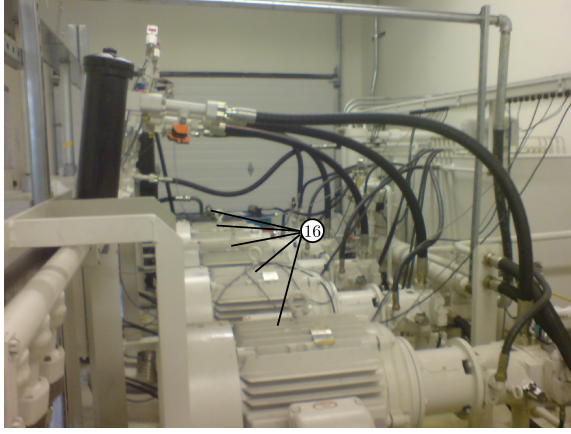
Figure 6.4: Pumping room. (16) Pumps that provides the flow to the system, (17) Lever that control the amount of water to the heat exchanger.

$$Q = nV \tag{6.1}$$

where Q is in liters per minute (lpm), n the pump speed in revolutions per minute (rpm) and V the displaced volume in cubic centimeters (cc). The number of pumps driving the flow are chosen based on the maximum amount of flow a pump can provide.

The temperature of the oil is controlled by a heating and cooling system which are located in the engine room. While running test rig the heating system are mainly used in the beginning to achieve the wished temperature at the inlet (LP port). The cooling system provides water to a heat exchanger that is cooling the oil. The amount of water to the heat exchanger are controlled by a lever(17) to a water pipe, see Figure 6.4. To keep a constant temperature in the inlet, this needs to be changed continuously during the tests. It is very crucial that the operator of the test rig control the flow of water until steady state is achieved for each measurement. To get a good measure point a number of measurements should be made for each point.

6.2   Case temperature model

The total energy dissipated in the three gaps and case can be formulated as

$$q_{gaps} = \mu \Phi_{gaps} V = \underbrace{\mu \Phi_{P/C} V_{P/C}}_{q_{P/C}} + \underbrace{\mu \Phi_{S/Sp} V_{S/Sp}}_{q_{S/Sp}} + \underbrace{\mu \Phi_{Cb/Vp} V_{Cb/Vb}}_{q_{Cb/Vp}} + \underbrace{\mu \Phi_{Churning} V_{Case}}_{q_{Churning}} \tag{6.2}$$

where V is the total volume of fluid trapped in the gaps and in the case. The energy dissipated in the case and for each gap are calculated separately and are then inserted into Equation 6.2.

Equation 3.39 or 3.40 are going to be solved in the three gaps and in the case. the gradients of the velocities are solved by applying the Navier-Stokes (N-S) equations in the gaps.

$$\rho \frac{\partial u_i}{\partial t} + \rho \frac{\partial u_i u_j}{\partial x_j} = -\frac{\partial p}{\partial x_i} + \mu \frac{\partial^2 u_i}{\partial x_j \partial x_j} \tag{6.3}$$

There are a some assumptions that can be made to simplify Equation 6.3. The first major assumption is to consider the height of the gaps to be constant. This makes the the pressure to only vary along the gaps, and the gradient of pressure is assumed to be

constant. The flow in the gaps is considered to be laminar and in steady-state, hence the time derivatives can be neglected. In lubricating gaps, the viscous forces dominates compared to the inertial forces, the left hand side in the N-S equations can therefore totally be neglected. The following sections will describe how the viscous dissipation is calculated in the case and in each gap.

6.3 Dissipation due to churning

The rotating motion of the cylinder block is churning the oil in the case, hence it is a source to the energy dissipated in the pump. The flow in the case are considered to only vary in the circumferential direction of the cylinder block, this is since the velocity gradient along the cylinder block are magnitudes of orders smaller. The pressure in the case is considered to be constant. The velocity field in the case can be seen in Figure 6.5.
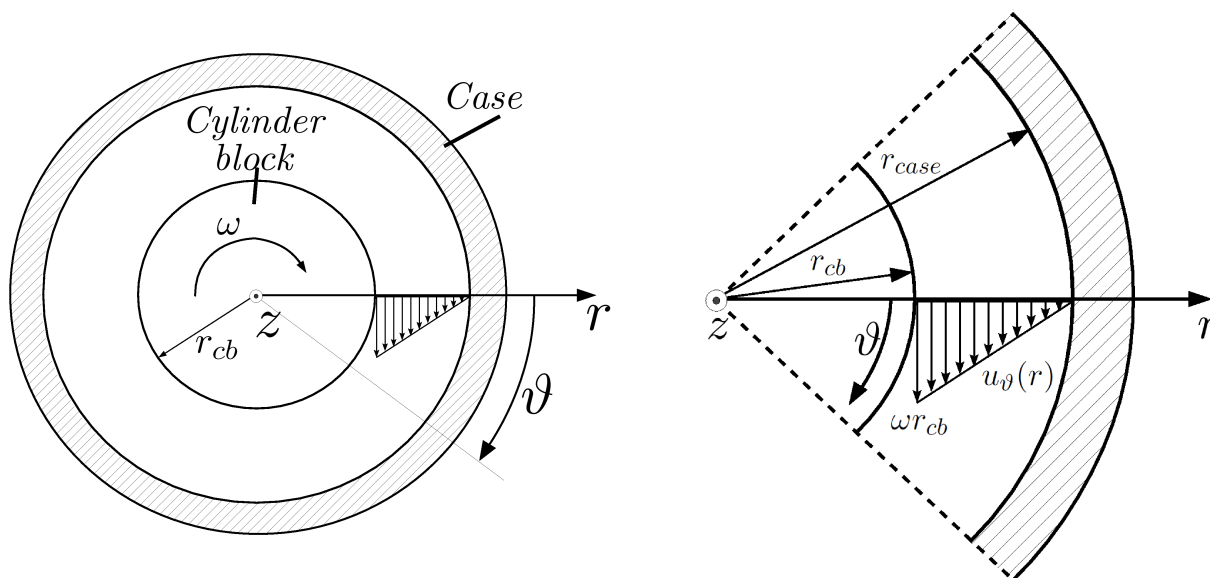
Figure 6.5: Velocity profile at a cross section in z-direction.

The flow in the case is treated as laminar. The assumptions in the case can be viewed below.

$$\frac{\partial u}{\partial r} >> \frac{\partial u}{\partial \vartheta}, \frac{\partial u}{\partial z} \qquad u_\vartheta >> u_z, u_r$$

The N-S equations in cylindrical polar coordinates can now be reduced to

(ϑ-direction)

$$0 = \mu \left[\frac{1}{r} \frac{\partial}{\partial r} \left(r \frac{\partial u_\vartheta}{\partial r} \right) - \frac{u_\vartheta}{r^2} \right] \qquad (6.4)$$

The boundary conditions in the case are

$$u_\vartheta(r_{case}) = 0 \qquad u_\vartheta(r_{cb}) = \omega r_{cb}$$

where r_{cb} is the radius of the cylinder block and r_{case} is the radius from the center of the cylinder block to the case. By integrate Equation 6.4 and using the boundary conditions the following expression for the velocity can be derived.

$$u_\vartheta = -\omega \frac{(r_{cb}/r_{case})^2}{1 - (r_{cb}/r_{case})^2} r + \omega \frac{r_{cb}^2}{(1 - (r_{cb}/r_{case})^2)r} \qquad (6.5)$$

The viscous dissipation equation in cylindrical polar coordinates can be reduced to

$$\mu\Phi_{Churning} = \mu\left(r\frac{\partial}{\partial r}\left(\frac{u_\vartheta}{r}\right)\right)^2 \tag{6.6}$$

To solve this equation, Equation 6.5 is modified and derivated

$$r\frac{\partial}{\partial r}\left(\frac{u_\vartheta}{r}\right) = -2\omega\frac{r_{cb}^2}{(1-(r_{cb}/r_{case})^2)r^2} \tag{6.7}$$

By inserting Equation 6.7 into Equation 6.6, the energy dissipated in the case can be calculated

$$q_{Churning} = \mu\Phi_{Churning}V_{Case} \tag{6.8}$$

6.4   Dissipation in the Piston/Cylinder interface

For the P/C interface, the following assumptions can be considered:

$$\frac{\partial u}{\partial z} >> \frac{\partial u}{\partial x}, \frac{\partial u}{\partial y} \qquad \frac{\partial p}{\partial x} >> \frac{\partial p}{\partial z}, \frac{\partial p}{\partial y} \qquad u_x, u_y >> u_z$$

The velocity profiles of the piston can then be considered as in Figure 6.6 and 6.7
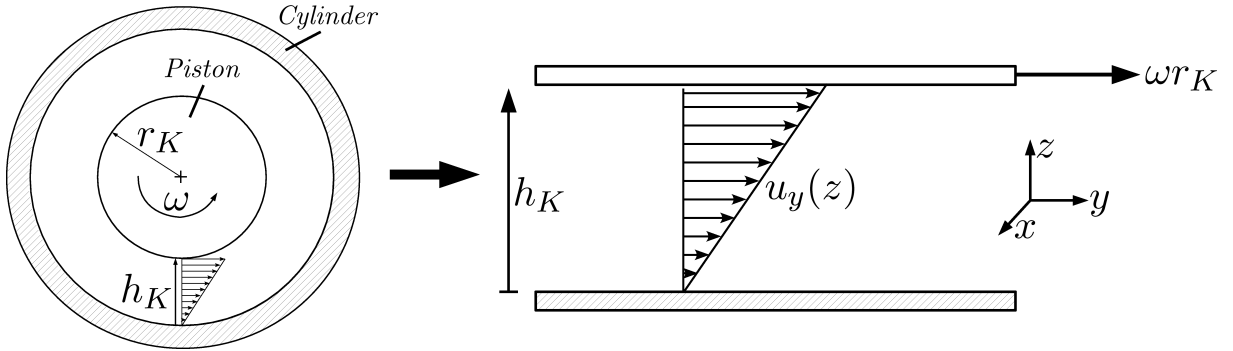
Figure 6.6: Velocity profile at a cross section in x-direction, treated in cartesian coordinates.

The clearance between the piston and cylinder is very small compared to the piston radius r_K, the curvature of the lubricant can be neglected and a cartesian coordinate system can be used.

The magnitude of the velocity gradients in the gap height direction (z-direction) is much larger than in the other directions. These assumptions reduces Equation 6.3 to

(x-direction)

$$0 = -\frac{\partial p}{\partial x} + \mu\frac{\partial^2 u_x}{\partial z^2} \tag{6.9}$$

(y-direction)

$$0 = \mu\frac{\partial^2 u_y}{\partial z^2} \tag{6.10}$$

The following boundary condition can be applied:

$$u_x(0) = 0 \qquad u_x(h_K) = v_K$$
$$u_y(0) = 0 \qquad u_y(h_K) = \omega r_K$$
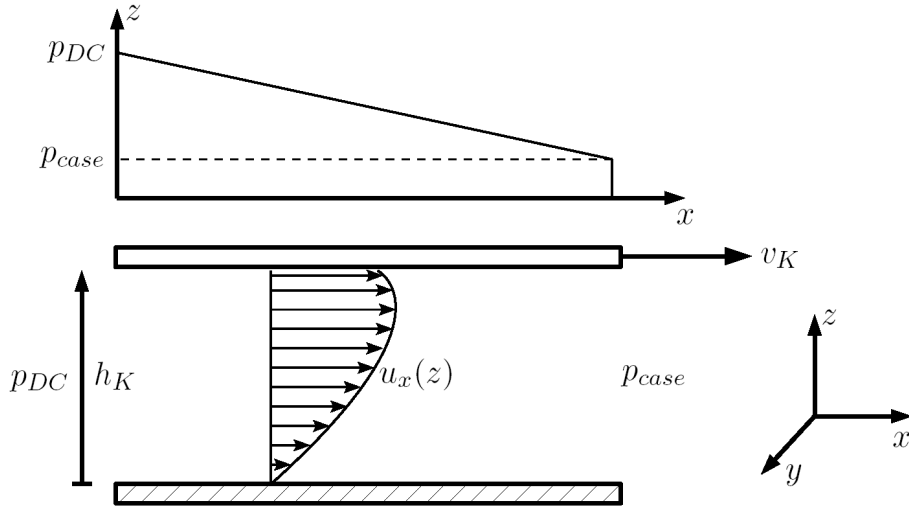
Figure 6.7: Velocity profile at a cross-section in y-direction along the gap.

Where r_K is the radius of the piston. With these boundary conditions, Equation 6.9 and Equation 6.10 can be integrated to

$$u_x = \frac{1}{2\mu}\frac{\partial p}{\partial x}\left(z^2 - zh_K\right) + \frac{v_K}{h_K}z \tag{6.11}$$

$$u_y = \omega r_K \frac{z}{h_K} \tag{6.12}$$

By looking at the visous dissipation equation again, Equation 3.39 can also be reduced

$$\mu\Phi_{P/C} = \mu\left[\left(\frac{\partial u_x}{\partial z}\right)^2 + \left(\frac{\partial u_y}{\partial z}\right)^2\right] \tag{6.13}$$

This equation can be solved with the derived equations of The N-S. To be able to solve it, the derivative of Equations 6.14 and 6.15 are needed

$$\frac{\partial u_x}{\partial z} = \frac{1}{2\mu}\frac{\partial p}{\partial x}\left(2z - h_K\right) + \frac{v_K}{h_K} \tag{6.14}$$

$$\frac{\partial u_y}{\partial z} = \omega r_K \frac{1}{h_K} \tag{6.15}$$

The velocity v_K is depending on the rotational angle ϕ. Equation 6.14 is therefore integrated over the revolution time, T, in order to get the mean gradient over a revolution. The velocity field in the x-direction is not linear, hence the viscous dissipation equation has to be integrated in the gap height direction (z-direction).

$$\frac{1}{T}\int_0^T\int_0^{h_K}\mu\Phi_{P/C}\,dz\,dt = \frac{1}{T}\int_0^T\int_0^{h_K}\mu\left[\left(\frac{\partial u_x}{\partial z}\right)^2 + \left(\frac{\partial u_y}{\partial z}\right)^2\right]dz\,dt \tag{6.16}$$

The energy dissipated in the gap can then be calculated with Equation 6.17

$$q_{P/C} = n\frac{1}{T}\int_0^T\int_0^{h_K}\mu\Phi_{P/C}\,dz\,dt\,A_s \tag{6.17}$$

Where the area A_s is the surface area of the piston within the gap length and n is the number of pistons.

6.5 Dissipation in the Cylinder block/Valve plate interface

In order to be able to solve the velocity field analytically, the valve plate has to be simplified. The ports are treated to be merged into each other, hence creating a empty space that is symmetric, see Figure 6.8. This is since the velocity field in r-direction has to be treated as symmetric.
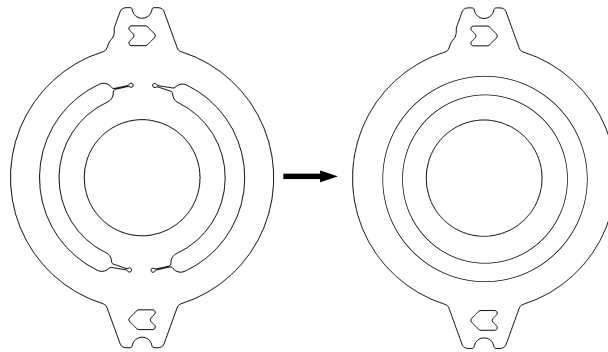
Figure 6.8: The original valve plate to the left are changed and is instead treated as the valve plate to the right

The local coordinate system in the Cb/Vp interface are treated in cylindrical polar coordinates, and it originates from a plane aligned with the surface of the valve plate, see Figure 6.9.
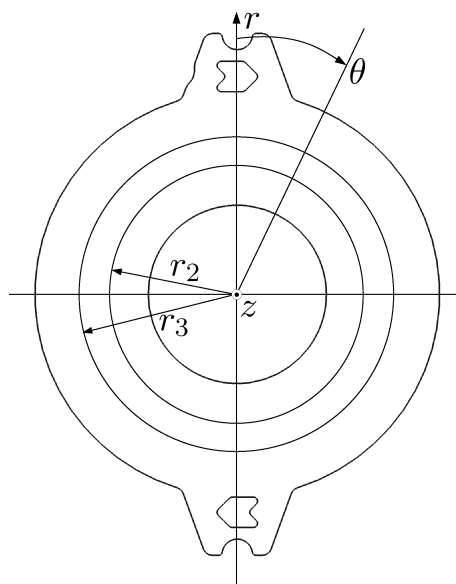
Figure 6.9: Coordinate system of the Cb/Vp interface (r, θ, z), with the dimensions: r_2, r_3

The cylinder block viewed from the valve plate side can be seen in Figure 6.10. Important to note here is that the viscous dissipation is created between the sealing land and the valve plate. The sealing land is the surface that is closest to the valve plate, hence constitute to the build of the lubricating gap.
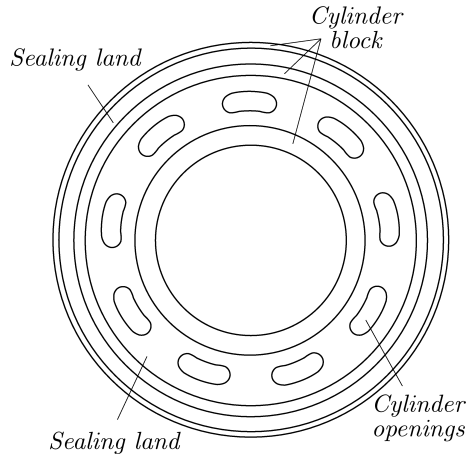
Figure 6.10: the parts of the cylinder block connected to the C/B interface

Since the port is merged into each other in the valve plate, the area between the cylinder openings at the sealing land surface is not contributing to the energy dissipated in the gap. This reduces the surface area of the sealing land to A_{s1}, A_{s2} and A_{s3}, see Figure 6.11.
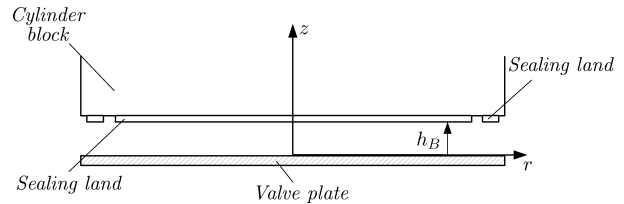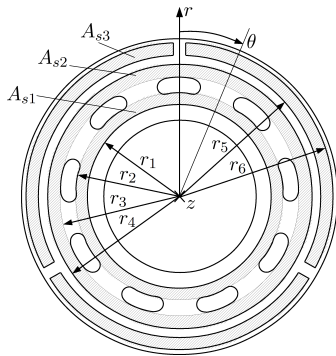
Figure 6.11: Dimensions of the cylinder block.

Figure 6.12: The gap in the C/B interface.

Figure 6.12 shows a side view of the cylinder block and valve plate interface, where the gap height is denoted as h_B.

The velocity field due to the rotation of the block is uniformly distributed in the gap (θ-direction). The rotational velocity can then be treated as a boundary condition that varies in r-direction. The following assumptions can then be considered.

$$\frac{\partial u}{\partial z} >> \frac{\partial u}{\partial r}, \frac{\partial u}{\partial \theta} \qquad \frac{\partial p}{\partial r} >> \frac{\partial p}{\partial z}, \frac{\partial p}{\partial \theta} \qquad u_r, u_\theta >> u_z$$

With these assumptions the N-S equations can be reduced to

(r-direction)

$$0 = -\frac{\partial p}{\partial r} + \mu \frac{\partial^2 u_r}{\partial z^2} \tag{6.18}$$

(θ-direction)

$$0 = \mu \frac{\partial^2 u_\theta}{\partial z^2} \tag{6.19}$$

to solve these equations, the following boundary conditions are applied

$$u_r(0) = 0 \qquad u_r(h_B) = 0$$
$$u_\theta(0) = 0 \qquad u_\theta(h_B) = \omega r$$

By integration and using the boundary conditions, the following equations for the velocities can be achieved

$$u_r = -\frac{1}{2\mu}\frac{\partial p}{\partial r}\left(z^2 - zh_B\right) \tag{6.20}$$

$$u_\theta = -\frac{1}{2\mu}\left(z^2 - zh_B\right) + \frac{\omega r}{h_B}z \tag{6.21}$$

The viscous dissipation can be reduced to the following equation with the given assumption

$$\mu\Phi_{Cb/Vp} = \mu\left[\left(\frac{\partial u_r}{\partial z}\right)^2 + \left(\frac{\partial u_\theta}{\partial z}\right)^2 + 2\left(\frac{u_r}{r}\right)^2\right] \tag{6.22}$$

The last term is orders of magnitude smaller than the gradients in the z-direction, hence Equation 6.22 can be reduced to

$$\mu\Phi_{Cb/Vp} = \mu\left[\left(\frac{\partial u_r}{\partial z}\right)^2 + \left(\frac{\partial u_\theta}{\partial z}\right)^2\right] \tag{6.23}$$

The velocity u_r is flowing in opposite directions from the port into the case, as explained with the leakage flow for the block in Section 3.2. Figure 6.13 and Figure 6.14 displays how the velocity profiles is considered in the Cb/Vp interface
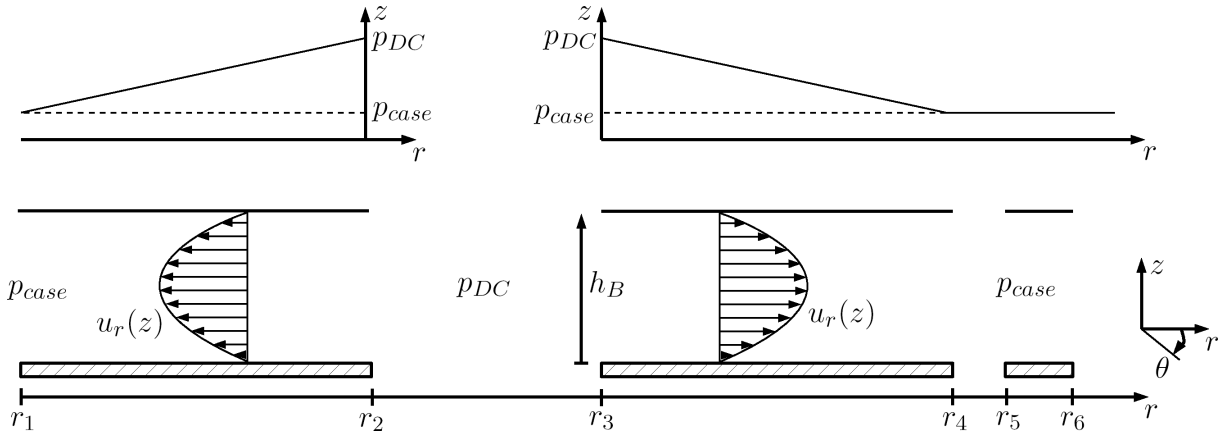
Figure 6.13: Velocity profile in the Cylinder block/Valve plate interface at a cross-section in θ-direction.

There is only contributions to the viscous dissipation at the surfaces A_{s1}, A_{s2} and A_{s3}. The viscous dissipations are created at different surfaces hence the different areas must be considered. Equation 6.23 is therefore integrated over the radius of the gap.

$$\mu\int_{r_1}^{r_6}\Phi_{Cb/Vp}2\pi r\,dr = \mu\int_{r_1}^{r_6}\left[\left(\frac{\partial u_r}{\partial z}\right)^2 + \left(\frac{\partial u_\theta}{\partial z}\right)^2\right]2\pi r\,dr \tag{6.24}$$

The first term in Equation 6.24 is rewritten to
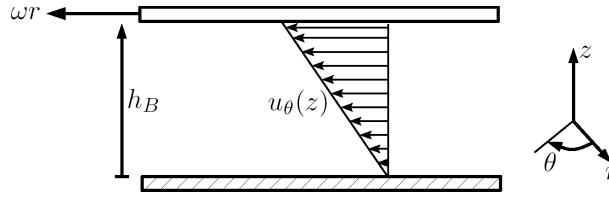
Figure 6.14: Velocity profile in the Cylinder block/Valve plate interface at a cross-section in r-direction.

$$\int\limits_{r_1}^{r_6} \left(\frac{\partial u_r}{\partial z}\right)^2 2\pi r\, dr = \int\limits_{r_1}^{r_2} \left(\frac{\partial u_r}{\partial z}\right)^2 2\pi r\, dr + \underbrace{\int\limits_{r_2}^{r_3} \left(\frac{\partial u_r}{\partial z}\right)^2 2\pi r\, dr}_{=0} +$$

$$+ \int\limits_{r_3}^{r_4} \left(\frac{\partial u_r}{\partial z}\right)^2 2\pi r\, dr + \underbrace{\int\limits_{r_4}^{r_6} \left(\frac{\partial u_r}{\partial z}\right)^2 2\pi r\, dr}_{=0} \qquad (6.25)$$

$$= A_{s1} \left(\frac{\partial u_r}{\partial z}\right)^2 \Big|_{s1} + A_{s2} \left(\frac{\partial u_r}{\partial z}\right)^2 \Big|_{s2}$$

since the pressure is constant in the port for an instant of time, the second term in the right hand side is considered to be zero. The same assumption applies where the radius is larger than r_4, since the pressure in the case is constant. The gap between r_5 and r_6 is only contributing to the viscous dissipation due to the rotation of the cylinder block.

The second term in Equation 6.24 is treated in a similar manner. The second term is integrated as

$$\int\limits_{r_1}^{r_6} \left(\frac{\partial u_\theta}{\partial z}\right)^2 2\pi r\, dr = A_{s1} \left(\frac{\partial u_\theta}{\partial z}\right)^2 \Big|_{s1} + A_{s2} \left(\frac{\partial u_\theta}{\partial z}\right)^2 \Big|_{s2} + A_{s3} \left(\frac{\partial u_\theta}{\partial z}\right)^2 \Big|_{s3} \qquad (6.26)$$

The rotation of the cylinder block is contributing to the viscous dissipation where the surface areas A_{s1}, A_{s2} and A_{s3} is existing, which is the whole surface of the gap.

The gradients of the velocities is achieved by derivate Equations 6.20, 6.21

$$\frac{\partial u_r}{\partial z} = -\frac{1}{2\mu}\frac{\partial p}{\partial r}\left(2z - h_B\right) \qquad (6.27)$$

$$\frac{\partial u_\theta}{\partial z} = -\frac{1}{2\mu}\left(2z - h_B\right) + \frac{\omega r_m}{h_B} \qquad (6.28)$$

Inserting Equations 6.27, 6.28 into Equation 6.24 and integrating over the gap height will give the energy dissipated in the gap

$$q_{Cb/Vp} = \frac{1}{T} \int\limits_0^T \int\limits_0^{h_B} \int\limits_{r_1}^{r_6} \mu \Phi_{Cb/Vp} 2\pi r\, dr dz dt A_s =$$

$$= \frac{1}{T} \int\limits_0^T \int\limits_0^{h_B} \mu \left[\int\limits_{r_1}^{r_6} \left(\frac{\partial u_r}{\partial z}\right)^2 2\pi r\, dr + \int\limits_{r_1}^{r_6} \left(\frac{\partial u_\theta}{\partial z}\right)^2 2\pi r\, dr A_s\right] dz dt \qquad (6.29)$$

Where A_s is the sum of the areas A_{s1}, A_{s2} and A_{s3}.

6.6 Dissipation in the Slipper/Swash plate interface

The S/Sp interface is the most complicated interface when considering the viscous dissipation calculation. The Slipper can rotate around its own axis. There are also velocity contributions due to the sliding motion that is created by the rotation around the shaft.

Figure 6.15 shows how the slipper is rotating around two axis.

Figure 6.15: Slipper rotation around the two centers, O and O_G.

The angular rotation of the slipper is considered to be the same as the shaft speed but with opposite sign, hence $\omega_G = -\omega$.

The resultant velocity V_G is divided into two components, V_{Ga} and $V_{G\gamma}$. The V_{Ga} are in the radial direction a, while $V_{G\gamma}$ are in the angular direction,γ. The slipper velocities in every point in (a,γ) are

$$
\begin{aligned}
V_{Ga} &= \omega r_M \cos \delta \\
V_{G\gamma} &= \omega (r_M \sin \delta - a)
\end{aligned}
\tag{6.30}
$$

Where component $V_{G\gamma}$ is the relative velocity around its center, O_G.

The resultant velocity is

$$
|V_G| = \sqrt{(\omega r_M \cos \delta)^2 + (\omega (r_M \sin \delta - a))^2} = \sqrt{\omega^2 (r_M^2 + a^2 - 2ar_M \sin \delta)} = \omega R_\phi \tag{6.31}
$$

This proofs that the the slipper is translating around the center O with a uniform velocity of ωR_ϕ. The velocity components are different around the slipper, this will change the gradient in the gap height direction (z-direction) in every point around the slippers, γ direction. The radius r_M is calculated at every point around the slipper.

$$r_M = \sqrt{R_\phi^2 + a^2 - 2aR_\phi \cos(180 - \gamma)} \tag{6.32}$$

$$R_\phi^2 = (R_B \sin \phi)^2 + \left(\frac{R_B \cos \phi}{\cos \beta}\right)^2 \tag{6.33}$$

Where R_B is the pitch radius of the pump and R_ϕ the radius to the center of the slipper, O_G, that varies with the rotating angle ϕ.

The pressure built up in the slipper is different from the pressure in the displacement chamber, hence this needs to be calculated.

The pressure built up is depending on the force that is pushing the slipper against the swash plate, F_{KS}, see Figure 6.16.
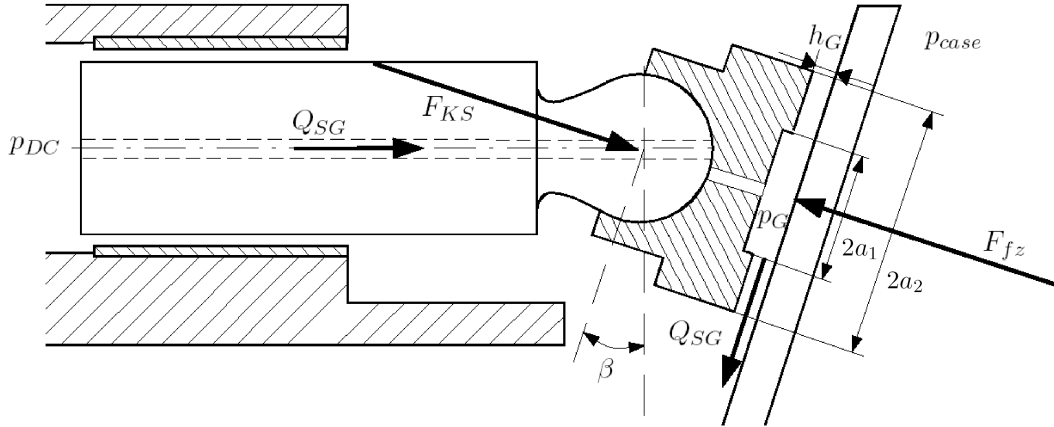
Figure 6.16: schematic of the slipper.

A responding force from the pressurized fluid in the slipper will push the slipper at the opposite direction, hence balancing the external forces. The load ability, F_{fz}, is described as

$$F_{fz} = \frac{1}{2}p_G\pi\frac{a_2^2 - a_1^2}{\ln\frac{a_2}{a_1}} \tag{6.34}$$

This fluid force is however lower than the external force F_{KS}, because there is also an contribution from the hydrodynamic pressure. Since the gap height is assumed to be constant in this case, the contribution from the hydrodynamic force is neglected. By neglecting this, the pocket pressure will be overestimated. To cover this, the contribution from the fluid force is assumed to be slightly lower.

$$F_{fz} = B_G F_{KS} \tag{6.35}$$

The constant B_G is between $0.95 - 0.99$, depending on the magnitude of the fictitious hydrodynamic force. The pressure in the slipper can then be described as

$$p_G = \frac{2F_{KS}\ln\frac{a_2}{a_1}}{\pi(a_2^2 - a_1^2)}B_G \tag{6.36}$$

The constant is used even with a constant gap height to avoid an over estimation in the pocket pressure.

The following assumptions can be considered in the lubricating gap for the slipper.

$$\frac{\partial u}{\partial z} >> \frac{\partial u}{\partial a}, \frac{\partial u}{\partial \gamma} \qquad \frac{\partial p}{\partial a} >> \frac{\partial p}{\partial z}, \frac{\partial p}{\partial \gamma} \qquad u_a, u_\gamma >> u_z$$

The velocity profiles of the slipper can then be considered as in Figure 6.17

(a) Velocity profile at a cross-section in γ-direction.

(b) Velocity profile at a cross-section in a-direction.
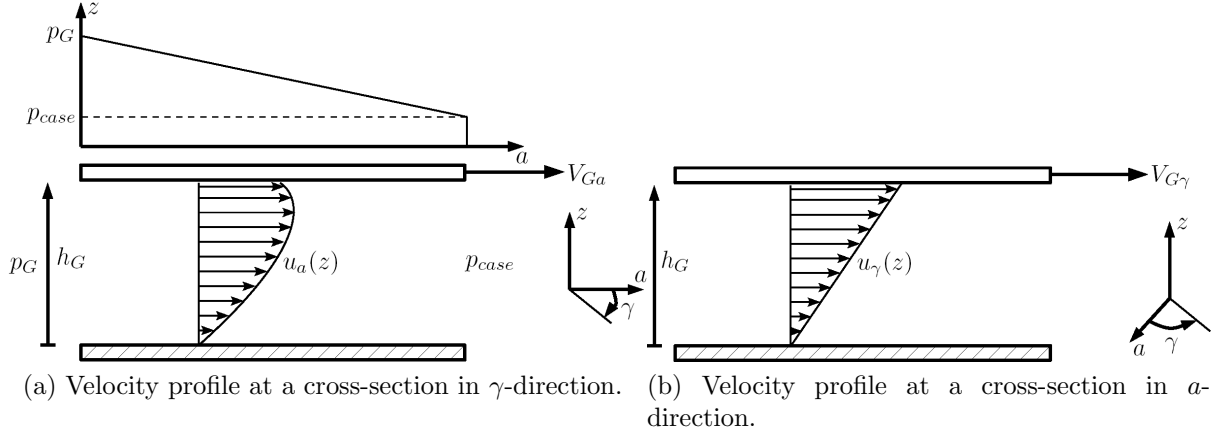
Figure 6.17: Assumed velocity profiles in the Slipper/Swash plate interface

The assumptions reduces the N-S equations to

$$0 = -\frac{\partial p}{\partial a} + \mu \frac{\partial^2 u_a}{\partial z^2} \qquad (6.37)$$

$$0 = \mu \frac{\partial^2 u_\gamma}{\partial z^2} \qquad (6.38)$$

by using the following boundary conditions

$$u_a(0) = 0 \qquad u_a(h_G) = V_{Ga}(a, \gamma, \phi)$$
$$u_\gamma(0) = 0 \qquad u_\gamma(h_G) = V_{G\gamma}(a, \gamma, \phi)$$

integration of Equations 6.37, 6.38 in the same manner as for the other interfaces, will give the equations for the velocities

$$u_a = -\frac{1}{2\mu} \frac{\partial p}{\partial a} \left(z^2 - z h_G \right) + \frac{V_{Ga}(a, \gamma, \phi)}{h_G} z \qquad (6.39)$$

$$u_\gamma = -\frac{1}{2\mu} \left(z^2 - z h_G \right) + \frac{V_{G\gamma}(a, \gamma, \phi)}{h_G} z \qquad (6.40)$$

Figure 6.18 shows how u_a and u_γ varies with γ at $z = h_G$, $a = \bar{a}$ and at $y = \overline{R_\phi}$.

The equation for the viscous dissipation can be reduced to the following equation with the given assumption

$$\mu \Phi_{S/Sp} = \mu \left[\left(\frac{\partial u_a}{\partial z} \right)^2 + \left(\frac{\partial u_\gamma}{\partial z} \right)^2 + 2 \left(\frac{u_a}{a} \right)^2 \right] \qquad (6.41)$$

In the same way as for the Cb/Vp interface, the last term is orders of magnitude smaller than the gradients in the z-direction, hence Equation 6.41 can be reduced to

$$\mu \Phi_{S/Sp} = \mu \left[\left(\frac{\partial u_a}{\partial z} \right)^2 + \left(\frac{\partial u_\gamma}{\partial z} \right)^2 \right] \qquad (6.42)$$

The derivatives of the velocities are obtained as

(a) The radial velocity u_a (b) The angular velocity u_γ

Figure 6.18: Normalized velocities at $z = h_G$
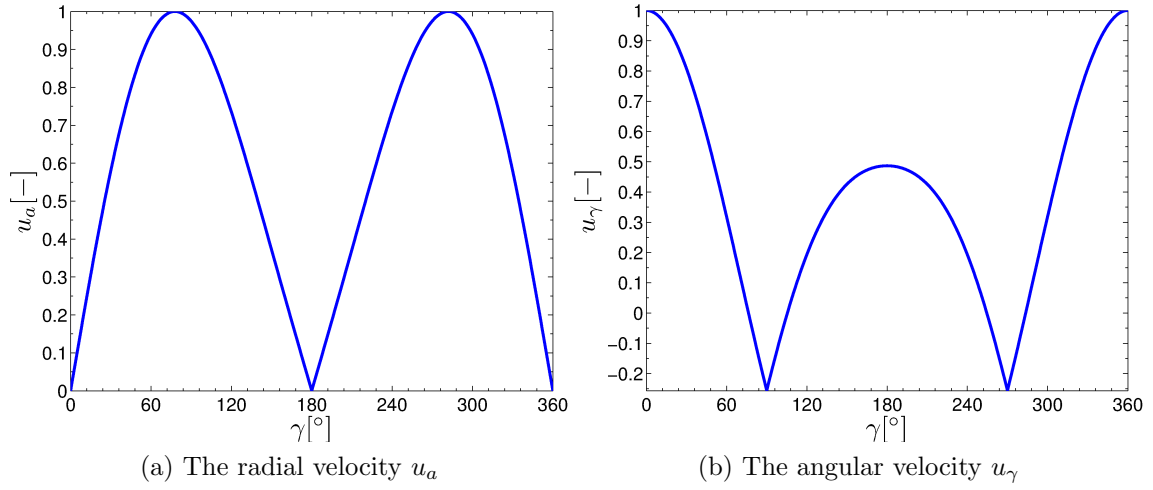
$$\frac{\partial u_a}{\partial z} = -\frac{1}{2\mu}\frac{\partial p}{\partial a}\left(2z - h_G\right) + \frac{V_{Ga}(a,\gamma,\phi)}{h_G} \tag{6.43}$$

$$\frac{\partial u_\gamma}{\partial z} = -\frac{1}{2\mu}\left(2z - h_G\right) + \frac{V_{G\gamma}(a,\gamma,\phi)}{h_G} \tag{6.44}$$

The velocity components of the slipper varies with a-,γ- and ϕ-direction. The viscous dissipation is integrated over a, γ the time it takes for the slipper to rotate around O in one revolution. This is in order to get a mean value of the viscous dissipation.

Inserting Equations 6.43 and 6.44 into Equation 6.42 and integrating over the gap height, radius, angle and time will give

$$\frac{1}{T\Gamma A}\int\limits_0^{h_G}\int\limits_0^T\int\limits_0^\Gamma\int\limits_{a_1}^{a_2}\mu\Phi_{S/Sp}\,da\,dt\,d\gamma\,dz = \frac{1}{T\Gamma A}\int\limits_0^{h_G}\int\limits_0^T\int\limits_0^\Gamma\int\limits_{a_1}^{a_2}\mu\left[\left(\frac{\partial u_a}{\partial z}\right)^2 + \left(\frac{\partial u_\gamma}{\partial z}\right)^2\right]da\,dt\,d\gamma\,dz \tag{6.45}$$

where the time T is the time it takes for the slipper to rotate a revolution around O and Γ is the angle of a revolution around O_G. A is the the distance from a_1 to a_2.

The energy dissipated in the gap can then be calculated

$$q_{S/Sp} = n\frac{1}{T\Gamma A}\int\limits_0^{h_G}\int\limits_0^T\int\limits_0^\Gamma\int\limits_{a_1}^{a_2}\mu\Phi_{Cb/Vp}\,da\,dt\,d\gamma\,dz\,A_s \tag{6.46}$$

Summing all the energy dissipations will give the total energy dissipated in the pump, as Equation 6.2 states.

6.7 Calculate the case temperature

The model considers that there is one flow entering the pump and two flows leaving. One flow is leaving the pump at the outlet, where the other flow are the sum of all flows leaving the pump due to leakage. The energy source that is heating the fluid in the pump are due to the energy dissipated, represented as q_{tot}. A representation of the system can be seen in Figure 6.19.
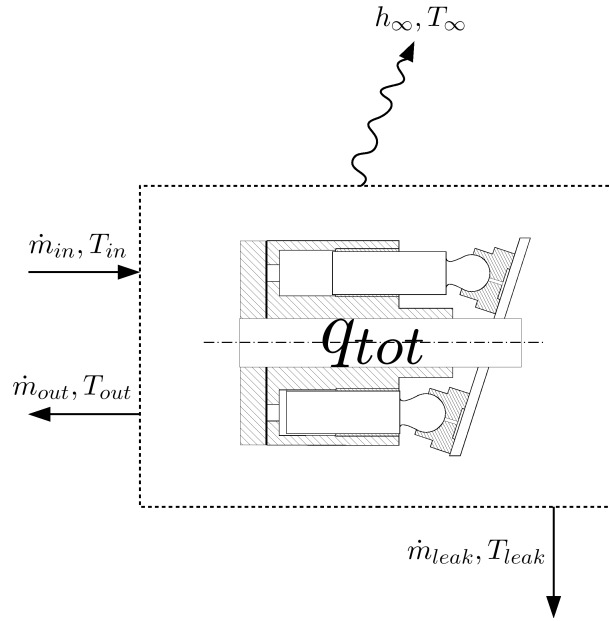
Figure 6.19: The system is represented as the control volume surrounding the pump.

The equations for the system are expressed as

$$\begin{cases} \dot{m}_{out}c_p(T_{out} - T_{in}) + \dot{m}_{leak}c_p(T_{leak} - T_{in}) + h_\infty A(T_{leak} - T_\infty) = q_{tot} \\ \dot{m}_{out} + \dot{m}_{leak} = \dot{m}_{in} \\ q_{tot} = q_{gaps} + q_{pump} \end{cases} \quad (6.47)$$

where the specific heat capacity, c_p, is treated as a constant. Equation 6.47 is solved and expressed in T_{leak} as

$$T_{leak} = \frac{q_{tot} - \dot{m}_{out}c_p(T_{out} - T_{in}) + \dot{m}_{leak}c_pT_{in} + h_\infty AT_\infty}{\dot{m}_{leak}c_p + h_\infty A} \quad (6.48)$$

The leakage temperature is determined as the amount of energy required to elevate the inlet temperature for a certain amount of mass flow through the gaps, $\dot{m}_{leak}$. The temperature of the flow leaving the pump is not only elevated because of the viscous dissipation in the gaps. The elevation of the outlet temperature is mostly elevated because of other effects in the pump, which is not included in the model. It is not trivial or even possible to determine the amount of energy that is rising the temperature of the outlet due to the other effects with a analytical model. Equation 6.48 is therefore modified.

The nominator in Equation 6.48 represents the amount of energy that rises the temperature in the leakage. The energy dissipated in the gaps are assumed to only heating the leakage flows, hence the outlet and the energy dissipated due to other effects are neglected.

$$T_{leak} = \frac{q_{gaps} + \dot{m}_{leak}c_pT_{in} + h_\infty AT_\infty}{\dot{m}_{leak}c_p + h_\infty A} \quad (6.49)$$

The total mass flow of the leakage is determined as

$$\dot{m}_{leak} = \rho(p,T)Q_{leak} = \rho(p,T)\left(\overline{Q}_{SK} + \overline{Q}_{SB} + \overline{Q}_{SG}\right) \quad (6.50)$$

The leakages from each gap is calculated as a mean value over a revolution. These values are achieved by integrate Equations 3.25, 3.30 and 3.27 over the revolution time

$$
\begin{cases}
\overline{Q}_{SK} = \frac{1}{T_0} \int\limits_0^{T_0} Q_{SK}(\phi)\, dt \\[2ex]
\overline{Q}_{SB} = \frac{1}{T_0} \int\limits_0^{T_0} Q_{SB}(\phi)\, dt \\[2ex]
\overline{Q}_{SG} = \frac{1}{T_0} \int\limits_0^{T_0} Q_{SG}(\phi)\, dt
\end{cases}
\tag{6.51}
$$

The leakages depends on the density of the fluid. The viscous dissipation depends on the viscosity which also depends on the pressure and temperature. The density and viscosity is not constant since the pressure and temperatures changes. Even if the fluid is regarded as incompressible, the compressible effects are still considered by determine the viscosity and density based on pressure and temperature. The kinematic viscosity is calculated by the following empirically determined equation for hydraulic fluids [2].

$$
\nu(p,T) = w e^{P_{c1}p T^{P_{c2}}} (10^{10^{(Tc1-Tc2*log10(T))}} - 0.5)10^{-6} \tag{6.52}
$$

The pressure and temperature of the gap is denoted as p and T. The pressure and temperature are consider to vary linearly over the gap, hence a mean value can be used. The weighting factor, w, is empirically determine depending on which type of hydraulic oil. The variables T_{c1}, T_{c2} and P_{c1}, P_{c2} are the temperature and pressure coefficients respectively. The coefficients are determined to match the behavior of the kinematic viscosity for the corresponding oil.

The density is calculated according to the following linear approximation [2]

$$
\rho(p,T) = \rho_0 \left[1 + \beta_p(p - p_0) - \beta_T(T - T_0)\right] \tag{6.53}
$$

where ρ_0 and T_0 is the reference density and temperature. The coefficients, β_p and β_T, are the isothermal coefficient of compressibility and the isobaric thermal coefficient of volumetric expansion, respectively.

The dynamic viscosity can then be calculated as:

$$
\mu = \nu \rho \tag{6.54}
$$

The viscosity and density are based on a mean value that is dependent on the leakage temperature. The calculation procedure for the leakage temperature requires an iteration process until the correct viscosity and density are achieved. The error for the temperature are defined as

$$
f = |T^{n-1} - T^n| \tag{6.55}
$$

where convergence is achieved if $f < 10^{-2}$. The flow chart in Figure 6.20 describes the calculation procedure.
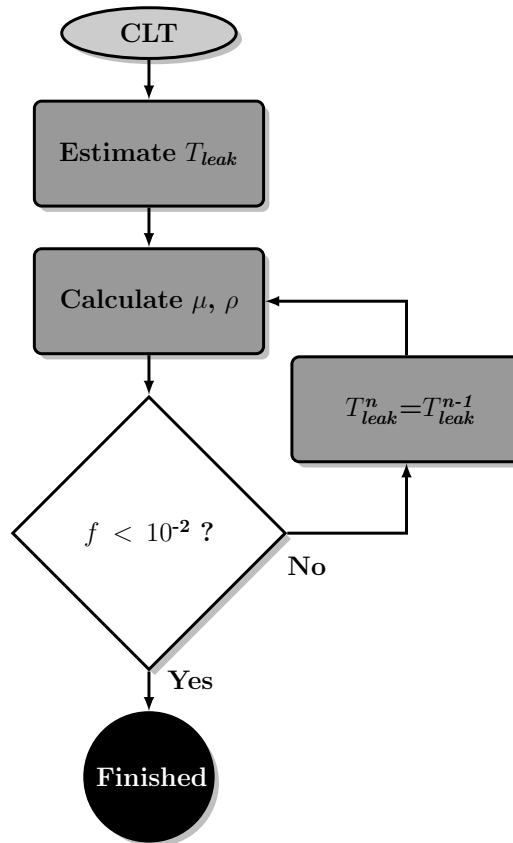
Figure 6.20: Flow chart of the calculation of leakage temperature (CLT)

7 Results

The result are presented in two parts, one for the CGFM and one for the case temperature. The results from the CGFM are primarily to show how the transfer of frictional forces have an impact on the power loss. The model for the case temperature is going to be compared to measured data and calculation with different gap heights has been performed in order to investigate the impact on the case temperature.

All simulations have been made for a *Sauer-Danfoss* 75cc pump with HLP 32 mineral oil.

7.1 CGFM

The tables presented in this section show how the volumetric efficiency and power loss changes with pressure and pump speed.

Table 7.1: Pump speed 500 rpm

Δp[bar]	η_v[%]		P_{loss}[W]	
	No forces	Forces	No forces	Forces
100	98.8	98.7	**470**	**640**
200	98.5	98.7	**644**	**625**

Table 7.2: Pump speed 1500 rpm

Δp[bar]	η_v[%]		P_{loss}[W]	
	No forces	Forces	No forces	Forces
100	99.3	99.4	**2413**	**2428**
300	99.2	99.2	**2796**	**2853**

Table 7.3: Pump speed 3000 rpm

Δp[bar]	η_v[%]		P_{loss}[W]	
	No forces	Forces	No forces	Forces
100	99.5	99.5	**7342**	**7357**
300	99.4	99.4	**7469**	**7576**

The transmitted friction forces seems to become of less importance when the pump speed is increased. The forces has a large impact on the power loss when the pump speed and pressure is low. A larger pressure in the pump becomes of larger importance when the pump speed is increased compared to the lower pump pressure.

7.2 Case temperature

The measured data are first presented in order to later validate the calculations with the case temperature model.

7.2.1 Measurments

The measurements where made at five different pump speeds; 1000, 1500, 2000, 2500 and 3000 rpm, and three different pressures; 100, 200 and 300 bar. These points are a usual range of operating conditions for the Sauer-Danfoss 75cc, and the points where chosen with care to reduce the risk of damaging the pump, hence the minimum and maximum operating conditions where not used. The case temperature in the pump has been assumed to correspond to the measured leakage temperature after reaching steady state condition.

Table 7.4: Pump speed 1000 rpm

Δp[bar]	Q_{leak}[l/min]	Q_{out}[l/min]	T_{in}[°C]	T_{out}[°C]	T_{leak}[°C]
100	2.78	71.22	52.06	54.28	53.20
200	2.95	68.90	52.04	56.15	57.02
300	3.27	66.64	52.46	58.42	63.63

Table 7.5: Pump speed 1500 rpm

Δp[bar]	Q_{leak}[l/min]	Q_{out}[l/min]	T_{in}[°C]	T_{out}[°C]	T_{leak}[°C]
100	3.14	108.23	51.49	53.66	59.64
200	3.26	105.85	51.35	55.26	63.29
300	3.59	103.18	51.69	57.29	68.70

Table 7.6: Pump speed 2000 rpm

Δp[bar]	Q_{leak}[l/min]	Q_{out}[l/min]	T_{in}[°C]	T_{out}[°C]	T_{leak}[°C]
100	3.45	145.47	52.68	55.10	64.91
200	3.68	142.40	51.41	55.69	69.89
300	4.25	138.54	52.53	58.69	77.74

Table 7.7: Pump speed 2500 rpm

Δp[bar]	Q_{leak}[l/min]	Q_{out}[l/min]	T_{in}[°C]	T_{out}[°C]	T_{leak}[°C]
100	4.08	182.65	51.27	53.28	65.76
200	4.24	179.05	51.00	54.62	72.42
300	4.58	167.41	52.23	58.91	80.96

Table 7.8: Pump speed 3000 rpm

Δp[bar]	Q_{leak}[l/min]	Q_{out}[l/min]	T_{in}[°C]	T_{out}[°C]	T_{leak}[°C]
100	4.71	220.57	51.31	53.41	69.22
200	5.05	215.78	51.65	55.35	76.39
300	5.94	210.85	52.67	58.06	81.65

The trend in the measurements are a raised leakage temperature for an increased pump speed and pump pressure. The change in pressure seems to have a larger impact on the leakage temperature than the increase in pump speed.

The data are also presented in a map to easier see the variations in case temperature, see Figure 7.1.
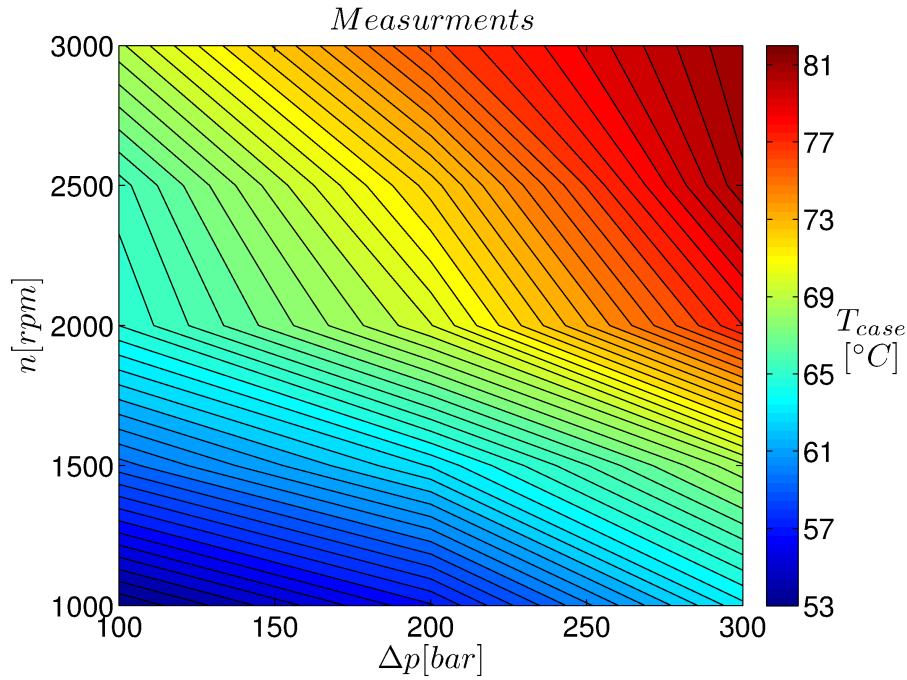
Figure 7.1: Case temperature map.

7.2.2 Case temperature model

The model has calculated the case temperature for five different pump speeds: 1000, 1500, 2000, 2500, 3000 rpm and three different pressures, 100, 200 and 300 bar with the maximum displacement at, $\beta = 17°$. The gap heights where set to: $h_K = 17\mu m$, $h_B = 8\mu m$, $h_S = 8\mu m$. Worth to note is that the gap height for the piston are calculated by subtracting the the radius of the piston from the radius of the bushing in the cylinder bore. The gap height for the Piston/Cylinder interface are also the interface which has the highest gap height, hence the gap heights tested for the Slipper/Swash plate and Cylinder block/Valve plate interface was smaller.

Table 7.9: Pump speed 1000 rpm

Δp[bar]	Q_{leak}[l/min]		q_{tot}[W]		T_{case}[°C]	
	calculated	measured	calculated	measured	calculated	measured
100	1.17	2.78	296.22	-	**57.83**	**53.20**
200	1.55	2.94	436.80	-	**59.94**	**57.02**
300	1.84	3.27	598.75	-	**62.27**	**63.63**

Table 7.10: Pump speed 1500 rpm

Δp[bar]	Q_{leak}[l/min]		q_{tot}[W]		T_{case}[°C]	
	calculated	measured	calculated	measured	calculated	measured
100	1.49	3.14	529.65	-	**63.00**	**59.64**
200	1.88	3.26	694.31	-	**64.26**	**63.29**
300	2.17	3.59	876.39	-	**66.09**	**68.70**

Table 7.11: Pump speed 2000 rpm

Δp[bar]	Q_{leak}[l/min]		q_{tot}[W]		T_{case}[°C]	
	calculated	measured	calculated	measured	calculated	measured
100	1.80	3.45	817.88	-	**67.85**	**64.91**
200	2.21	3.68	1014.31	-	**68.61**	**69.89**
300	2.51	4.25	1223.69	-	**70.13**	**77.74**

Table 7.12: Pump speed 2500 rpm

Δp[bar]	Q_{leak}[l/min]		q_{tot}[W]		T_{case}[°C]	
	calculated	measured	calculated	measured	calculated	measured
100	2.11	4.08	1151.23	-	**72.34**	**65.76**
200	2.54	4.24	1384.76	-	**72.79**	**72.42**
300	2.85	4.58	1626.61	-	**74.13**	**80.96**

Table 7.13: Pump speed 3000 rpm

Δp[bar]	Q_{leak}[l/min]		q_{tot}[W]		T_{case}[°C]	
	calculated	measured	calculated	measured	calculated	measured
100	2.41	4.71	1522.93	-	**76.49**	**69.22**
200	2.86	5.05	1797.76	-	**76.75**	**76.39**
300	3.20	5.94	2076.67	-	**77.99**	**81.65**

The case temperature is increasing for an increased pump speed and pump pressure. However the trend is not similar as the measured leakage temperature. The pressure has a larger impact on the case temperature for lower pump speeds compared to higher ones. This is a reversed behavior compared to the trend of the leakage temperatures, where large changes in pressure will raise the temperature even more for high pump speeds.

The model also under predicts the amount of leakage, which is strongly related to the gap heights.

To be able to determine how large impact the gap heights has on the temperature for a wider range of operating conditions, 1476 simulations where runned for each test of different gap heights. The results are expressed in the temperature maps below.

Gap heights of 10 μm and 12 μm for the slipper and cylinder block interface were also tested, see Figure 7.3 and 7.4

$$h_K = 17\mu m, \quad h_B = 8\mu m, \quad h_G = 8\mu m$$

Figure 7.2: Case temperature for gap heights: $h_K = 17\mu m$, $h_B = 8\mu m$, $h_S = 8\mu m$.

$$h_K = 17\mu m, \quad h_B = 10\mu m, \quad h_G = 10\mu m$$

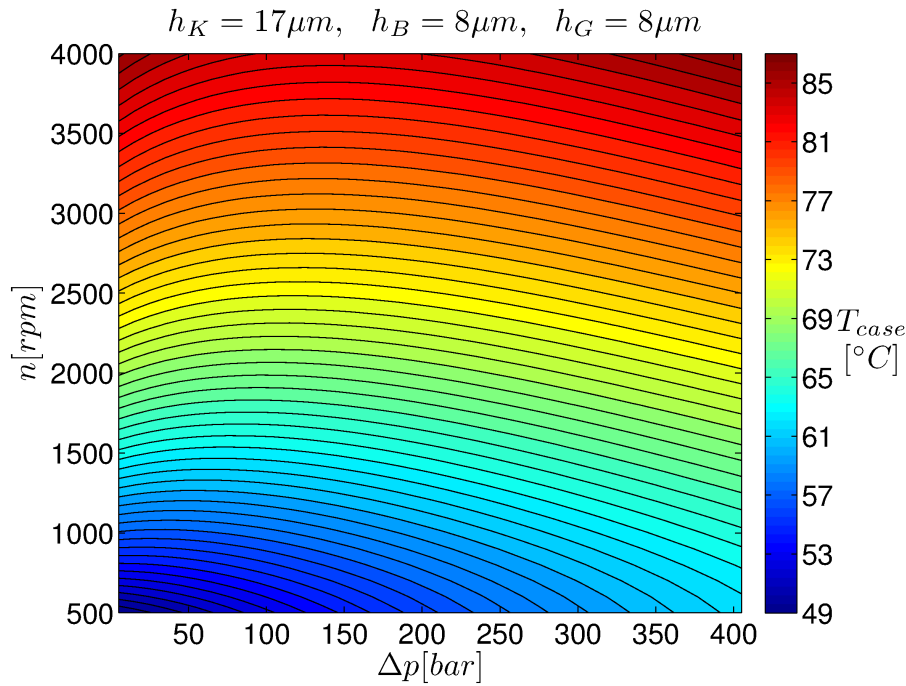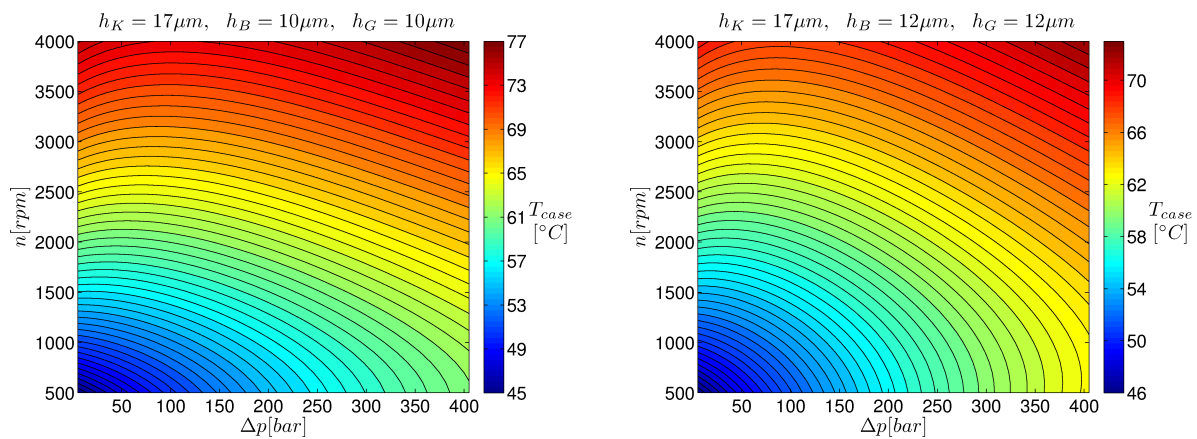$$h_K = 17\mu m, \quad h_B = 12\mu m, \quad h_G = 12\mu m$$

Figure 7.3: Case temperature for gap heights: $h_K = 17\mu m$, $h_B = 10\mu m$, $h_S = 10\mu m$.

Figure 7.4: Case temperature for gap heights: $h_K = 17\mu m$, $h_B = 12\mu m$, $h_S = 12\mu m$.

The gap heights have a large influence on the case temperature. To be able to get a better estimation of the case temperature, calculations from *CASPAR* have been done in order to get mean gap heights for different operating conditions for the slipper and cylinder block.

The gap heights has been loaded and used in the case temperature model with a result displayed in Figure 7.5.

The variation in case temperature as a dependency of gap heights can be viewed in Figure 7.6. This show how much the gap heights is able to raise the case temperature. The gap heights can be raised up to $40°C$ when going from 17 to 2 microns.
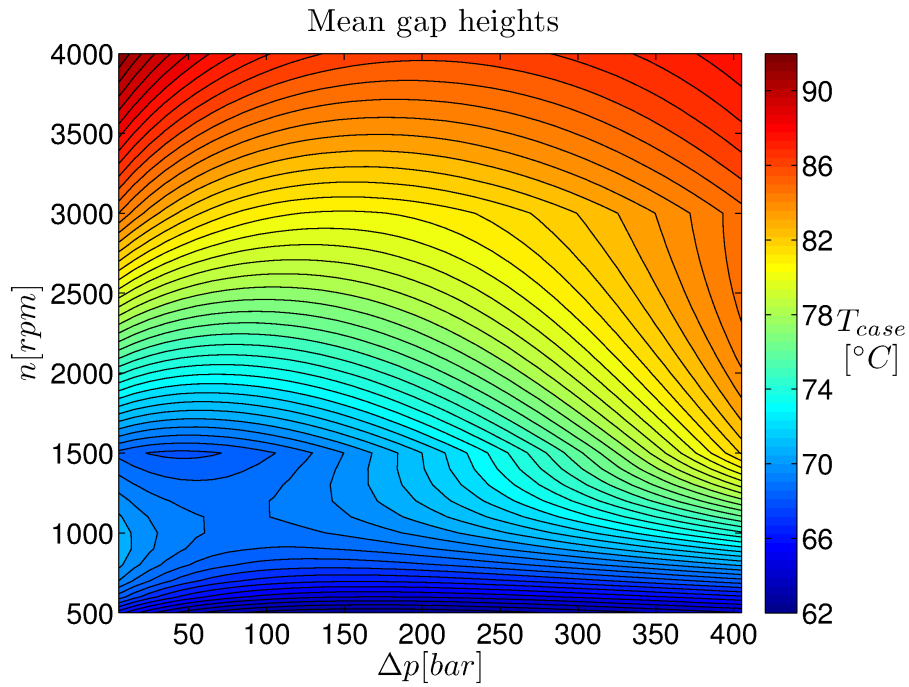
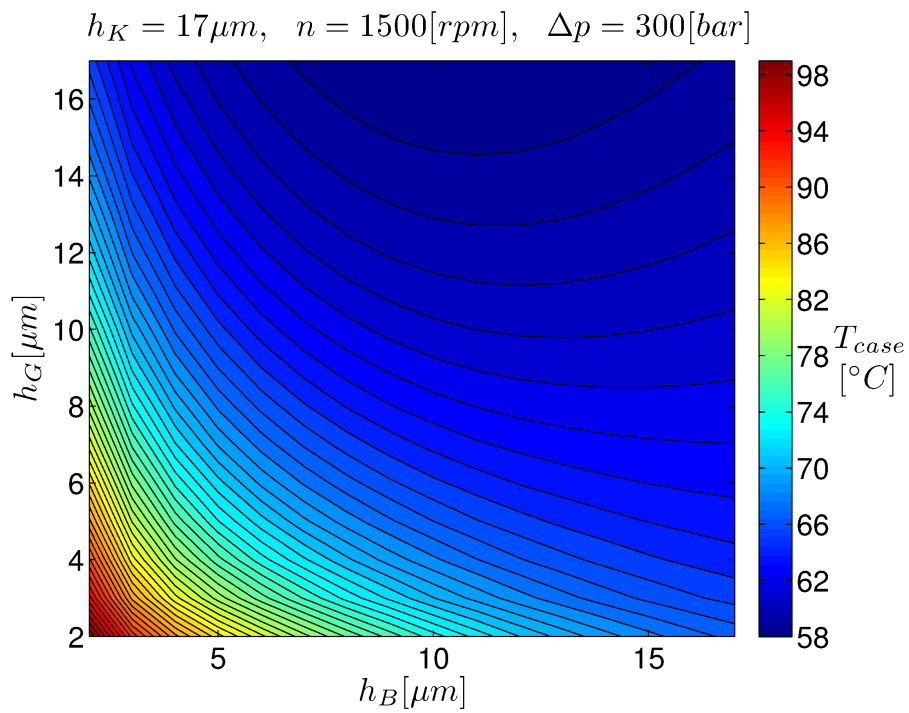Figure 7.5: Case temperature for mean gap heights from *CASPAR*.

Figure 7.6: Case temperature for variable gap heights for the cylinder block and slipper.

8 Summary and Conclusions

The friction forces transmitted in the *Coupled Gap Flow Module* have a larger impact on the power loss for low pump speeds with low pressures for a Sauer-Danfoss 75cc pump. This is since the other forces becomes much larger than the friction forces for higher pump speeds and pressures.

The volumetric efficiency is decreasing for increased pressures and is increasing for increased pump speeds. Compared with Figure 2.5 this agrees well when located at the left side where the slope is positive (in the graph to the right). This shows that the increase in leakage due to increased pressures are larger than the relative leakage increase due to higher pump speeds. This means that the leakage produced is becoming smaller for higher pump speeds relative the total flow through the pump.

The results from the model that predicts the case temperature has a trend to rise the temperature when the pump speed and pressure are increasing. The case temperature is strongly dependent on the gap heights and smaller gap heights increases the case temperature due to the increase in viscous dissipation in the gaps. The case temperature agrees well with the measurements for a pressure of 200 bar at the five different pump speeds when the gap heights are set to: $h_K = 17 \mu m$, $h_B = 8 \mu m$, $h_S = 8 \mu m$. However, since the gap heights are empirically chosen and its impact on the case temperature is high, the approximation to assume the gap heights to be constant is not a valid assumption.

The variable gap heights shown in Figure 7.5 is showing the case temperature with mean gap heights that was calculated with *CASPAR* for different pump speeds and pressures (note that the gap heights are still assumed to be constant for each pressure and pump speed). The case temperature is not agreeing well with the measurements, which gives a strong indication that the assumption to use constant gap heights are a too big approximation. Figure 7.6 shows how much the case temperature is varying for changes in gap heights for the slipper and cylinder block interfaces. The temperature was raised up to $40°C$ when changing the gap heights from 17 to 2 microns. It is therefore obvious that the gap heights is one of the largest source of the inaccuracy that the developed case temperature model produce.

9 Future Work

There may be several ways to improve the case temperature model, but one of the largest source of error in predicting the case temperature is the empirically chosen constant gap heights. A recommendation is therefore to integrate the case temperature model with *CASPAR* where the gap heights are calculated. To improve the prediction further is probably to develop a version of *CASPAR* which calculates the three gaps in one program instead of three separate ones. This will give a good indication if the case temperature can be calculated by only using the energy dissipated in the gaps.

References

[1] K. A. Edge and J. Darling. *Cylinder pressure transients in oil hydraulic pumps with sliding plate valves.* University of Bath, Bath, UK, 1986.

[2] A. Fredrickson and R. Klop. *User manual for CASPAR 2007 simulation program.* MAHA Fluid Power Research Center, Lafayette, US, 2007.

[3] J. Ivantysyn and M. Ivantysynova. *Hydrostatic pumps and motors.* Akademia Books International, New Delphi, India, 2001.

[4] R. Klop. *Investigation of Hydraulic Transmission Noise Source.* MAHA Fluid Power Research Center, Purdue University, West Lafayette, US, 2010.

[5] M. Pelosi. *An investigation on the Fluid-Structure Interaction of Piston/Cylinder Interface.* Purdue University, West Lafayette, US, 2011.

[6] U. Wieczorek. *An interpretation tool for axial piston machines of the swash plate design on basis of the computation of the gap flow.* Technical University of Hamburg, Hamburg, Germany, 2002.

[7] U. Wieczorek and M. Ivantysynova. *Computer Aided Optimization of Bearing and Sealing Gaps in Hydrostatic Machines - The Simulation Tool CASPAR.* International Journal of Fluid Power, Vol. 3 (2002), No.1, pp. 7-20., Hamburg, Germany, 2002.

[8] M. Zecchi. *Reynolds equation in CASPAR.* MAHA Fluid Power Research Center, Lafayette, US, 2010.